Journal of *Marine Science and Engineering*

MDPI

Article

Effect of Submarine Cables and Variable Bathymetry on Wave Energy Converter Park Optimization: A Genetic Algorithm Study in Todos Santos Bay, Mexico

Eduardo Santiago-Ojeda [1], Héctor García-Nava [2,*], Everardo Gutiérrez-López [3], Manuel Gerardo Verduzco-Zapata [4] and Gabriel García Medina [5]

[1] Facultad de Ciencias Marinas, Universidad Autónoma de Baja California, Carretera Ensenada-Tijuana No. 3917, Fraccionamiento Playitas, Ensenada 22860, Baja California, Mexico; santiago.eduardo@uabc.edu.mx
[2] Instituto de Investigaciones Oceanológicas, Universidad Autónoma de Baja California, Carretera Ensenada-Tijuana No. 3917, Fraccionamiento Playitas, Ensenada 22860, Baja California, Mexico
[3] Facultad de Ciencias, Universidad Autónoma de Baja California, Carretera Ensenada-Tijuana No. 3917, Fraccionamiento Playitas, Ensenada 22860, Baja California, Mexico; everardo.gutierrez@uabc.edu.mx
[4] Facultad de Ciencias Marinas, Universidad de Colima, Carretera Manzanillo-Cihuatlán Km 19.5, Colonia El Naranjo, Manzanillo 28868, Colima, Mexico; manuel_verduzco@ucol.mx
[5] Natural Systems Design, 1900 N. Northlake Way, Suite 211, Seattle, WA 98103, USA; gabriel.garcia@naturaldes.com
* Correspondence: hector.gnava@uabc.edu.mx

Abstract

Todos Santos Bay, Mexico, features several wave-focusing areas driven by its complex bathymetry, making it an ideal real-world test case for wave energy converter (WEC) park optimization. This study quantifies the influence of submarine cable costs and bathymetry-dependent mooring costs on the proposed park layout (hereafter the *star-layout*) and the levelized cost of energy (LCOE) of a 10-device WEC park, using a multi-state operational wave climatology of $N = 179$ representative sea states from a 2008–2018 SNL-SWAN hindcast (covering 97.20% of the annual time). A binary genetic algorithm combined with K-means clustering analysis was used to minimize LCOE under three cost scenarios: baseline, cable-only, and cable plus bathymetry-dependent mooring. Both infrastructure cost components contribute substantially: cable costs add 52.2% to the baseline LCOE, and bathymetry-dependent mooring costs add a further 16.0% at this site, with cable approximately three times more impactful. These quantitative magnitudes are conditioned on the moderate depth-gradient setting of Todos Santos Bay; the qualitative cost-component hierarchy is expected to generalize, but the relative weights will depend on the bathymetric and wave-climate characteristics of each candidate site. The mooring contribution is nontrivial both economically and spatially (the centroid of the park shifts by approximately 151 m between the cable-only and cable-plus-depth scenarios). K-means clustering identified 2–4 layout families per scenario ($K = 4 \rightarrow 3 \rightarrow 2$ as cost components are added), indicating that infrastructure constraints reduce the viable solution space. These results support the central hypothesis of this work: WEC park optimization studies that adopt flat-bathymetry simplifications, the prevailing assumption in much of the prior literature, risk substantial underestimation of LCOE at sites with nontrivial depth variation. We recommend that bathymetry-dependent mooring costs be included alongside cable costs in any early-stage techno-economic assessment of WEC parks at sites with complex bathymetry.

Keywords: wave energy converter; WEC park optimization; genetic algorithm; LCOE; bathymetry; Todos Santos Bay; offshore renewable energy

Received: 24 March 2026
Revised: 1 May 2026
Accepted: 8 May 2026
Published: 18 May 2026

1. Introduction

Wave energy converter (WEC) park placement directly affects the levelized cost of energy (LCOE) through both wave-power capture and infrastructure cost [1,2]. Yet most optimization studies assume a fundamental simplification: flat (constant depth) bathymetry. This assumption ignores two cost factors that depend directly on seafloor topography (submarine cable length and mooring system depth), leading to substantial underestimation of project costs and unreliable LCOE assessments that compromise early-stage investment decisions.

Several optimization approaches have been explored for WEC parks. State-of-the-practice reviews [3,4] show that classical deterministic methods, while accurate for small and simple layouts, become computationally intractable as problem complexity grows. The WEC park layout search space is non-convex and multimodal, and numerical methods based on boundary element models are typically limited to arrays of up to ten devices due to their high computational cost [4]. Computational intelligence approaches have consequently become the dominant paradigm, accounting for over 50% of layout optimization studies since 2015 [4]. Genetic algorithms in particular have proven effective for this multimodal optimization problem [5–8], and particle swarm optimization has been applied to hybrid wind-wave farms, where the discount rate dominated final costs [9]. Multi-objective approaches have also been developed to balance competing objectives such as power production, cable length, and foundation costs [7,8,10]. Notably, nearly all studies in these reviews assume flat bathymetry, a simplification we examine here.

Bathymetry influences LCOE through multiple mechanisms (available wave power, cost penalties, and energy transmission) and plays a critical role in site selection for marine energy devices [11,12]. However, few studies have incorporated real bathymetric data into optimization. Ref. [13] evaluated linear arrangements under real bathymetric conditions and found arrow-shaped layouts most efficient, but did not include depth-dependent mooring costs. Ref. [14] designed wave energy farms for real wave climates in the Italian offshore, demonstrating the importance of site-specific conditions. Whether cable length or water depth dominates LCOE optimization at sites with real bathymetry remains an open question.

Submarine cable distance refers to the total length of the electrical cable connecting the WEC park to the onshore substation; it scales linearly with the park's geographic position and is therefore a direct function of the layout. Water depth at each device location determines the required mooring line length and the complexity of the anchor system, increasing capital expenditure for deeper deployments. Both variables are governed by the layout coordinates, making them natural cost components in the optimization objective. Including them transforms a purely energy-based problem into a techno-economic one in which the optimal park location must balance wave resource availability against infrastructure constraints. Their relative importance is site-dependent and not a priori evident, since the spatial gradients of cable length and water depth depend on the specific bathymetric and geographic setting of each site, motivating the systematic comparison conducted in this study.

The present study addresses this gap using real bathymetric data from Todos Santos Bay, Mexico, a site with natural wave focusing that creates multiple local power maxima [15]. The aim is to quantify the relative importance of submarine cable costs and depth-dependent mooring costs in WEC park optimization, and to characterize the solution landscape through systematic genetic algorithm experiments combined with K-means clustering analysis. The quantitative findings reported here apply specifically to the bathymetric and wave-climate setting of Todos Santos Bay; the optimization framework itself is general and transferable to other sites with appropriate input data.

A genetic algorithm was proposed to optimize a 10-device WEC park under three progressive cost scenarios: energy-based LCOE only, LCOE with cable costs, and LCOE

with both cable and depth-dependent mooring costs. Each scenario was evaluated across 16 parameter combinations with 100 independent executions, yielding approximately 480 million total function evaluations across all configurations. K-means clustering was then applied to identify families of near-optimal layouts, providing insight into both the optimization landscape topology and the robustness of results.

We find that submarine cable costs are approximately three times more impactful than bathymetry-dependent mooring costs on LCOE (+52.2% for cable over the no-infrastructure baseline, +16.0% for depth-dependent mooring over the cable-only baseline), with both contributions remaining material rather than one being dominant and the other negligible. This cost-component hierarchy contradicts the common practice of using flat-bathymetry approximations and cable-only cost models for techno-economic assessment of WEC parks at sites with nontrivial depth variation.

The paper is organized as follows. Section 2 describes the study site and wave climate. Section 3 presents the methodology, including the LCOE formulation, genetic algorithm configuration, and clustering approach. Section 4 reports the optimization results and clustering analysis. Section 5 discusses the implications of the findings, and Section 6 provides conclusions and recommendations.

2. Study Site and Wave Climate

Evaluating the relative importance of cable costs and bathymetry-dependent mooring costs requires a site that combines bathymetric complexity with well-characterized wave conditions that have been found suitable for wave energy harvesting. Todos Santos Bay, Mexico, meets both criteria.

2.1. Todos Santos Bay, Mexico

Todos Santos Bay (Figure 1) provides an ideal testbed for evaluating bathymetry effects on WEC park optimization. The bay features San Miguel Reef, a submarine elevation that creates natural wave focusing through the combined effects of wave refraction and diffraction, a phenomenon that generates multiple local power maxima within a relatively small area. This bathymetric complexity, combined with proximity to potential grid connection points (marked with red X markers in Figure 1), makes it possible to directly compare scenarios where cable distance and water depth vary significantly across candidate park locations.

Previous studies have examined wave focusing and potential WEC sites in this region [15–17], establishing the wave climate characteristics. However, these studies focused on small parks or structural focalizers. A systematic optimization of WEC layouts across the full region has not yet been undertaken.

2.2. Wave Climate

The wave climate determines the spatial distribution of energy available for extraction, directly influencing optimal park locations. Based on the 10-year hindcast (2008–2018) of [15], Todos Santos Bay is characterized by swell-dominated conditions with a predominant wave direction from the northwest. Annual mean significant wave height is approximately 1.0–1.5 m, with peak periods ranging from 12–18 s. Wave energy is highest during winter months (November–March) due to North Pacific storm activity, with a domain-averaged mean power of approximately 9.9 kW/m, roughly twice the summer average (4.9 kW/m, June–September). The long-term mean wave power distribution (Figure 2) confirms that the highest energy levels occur along the western boundary of the domain, where swell arrives with minimal attenuation, and reveals localized energy focusing over the San Miguel Reef and Todos Santos North Island. The seasonal variability in wave power and peak direction is

summarized in Figure 3. The dominant peak direction remains near 353° (NNW) throughout the year, with a slight shift toward due north during summer months (July–September), reflecting the consistent North Pacific swell origin across seasons.

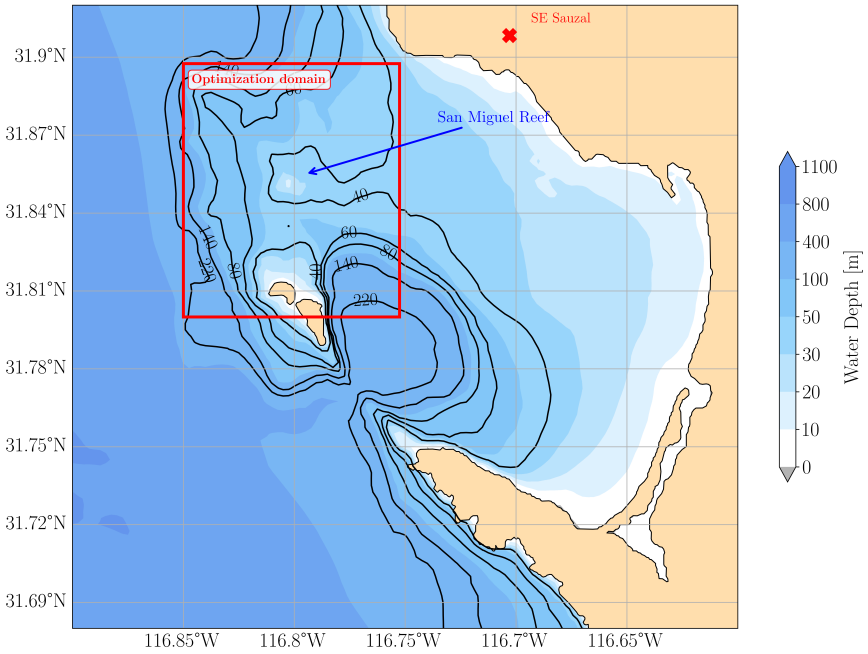

Figure 1. Bathymetry of the study area in Todos Santos Bay, Baja California, Mexico. The blue contours indicate water depth. The central feature is San Miguel Reef, with a depth of approximately 10 m at its shallowest point. The area with depths of less than 40 m is of particular interest due to wave-focusing effects. Red X markers indicate the locations of onshore substations for grid connection. The variable bathymetry in this region creates natural wave focusing, making it suitable for studying bathymetry effects on WEC park optimization.

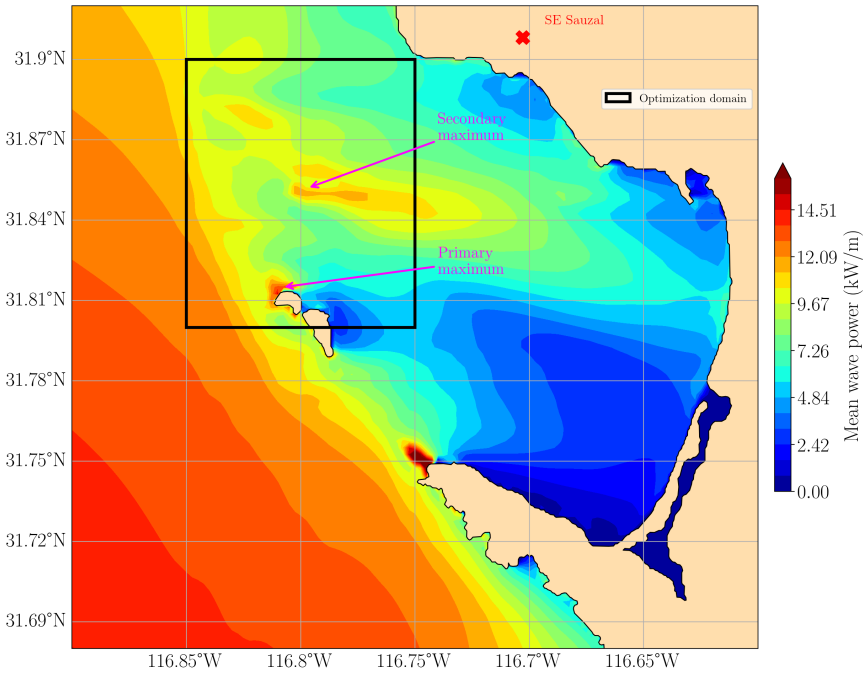

Figure 2. Mean wave power distribution in Todos Santos Bay computed from 10 years of SNL-SWAN hindcast simulations (2008–2018). Values represent the long-term mean wave power. The annual domain-averaged power is 7.5 kW/m. The black rectangle indicates the WEC park optimization domain, and the red cross marks the SE Sauzal electrical substation.

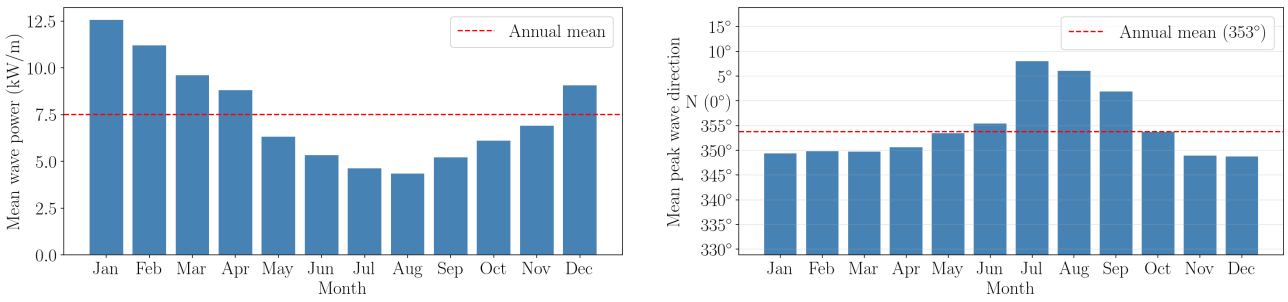

(**a**) (**b**)

Figure 3. Seasonal variability of wave power and peak direction in Todos Santos Bay based on the 2008–2018 SNL-SWAN hindcast, (**a**) Monthly mean wave power. (**b**) Monthly mean peak wave direction.

As shown in Figure 2, the wave power distribution in the optimization domain reveals a bimodal pattern with two distinct high-energy zones. This distribution creates competing attractors for the optimization algorithm: the primary maximum near the Todos Santos Islands and a secondary maximum over San Miguel Reef (both labeled in Figure 2). The relative influence between these power maxima and the cost gradients (cable distance, water depth) forms the core of the optimization challenge addressed in this study.

2.3. Bathymetric Data

The bathymetry of Todos Santos Bay used in this study is a composite of measurements and nautical chart data; it includes high-resolution measurements over some critical areas, such as the San Miguel bank and around Todos Santos Island. The bathymetry was interpolated to a computational grid of 257 × 257 nodes, covering the study domain (11.1 km × 9.4 km) used for the optimization experiments, resulting in a spatial resolution of 43.4 m (N–S) and 36.7 m (E–W).

3. Methodology

The non-convex and multimodal nature of the WEC park layout optimization problem [4], intensified here by the multiple local power maxima generated by Todos Santos Bay's complex bathymetry, renders classical deterministic methods computationally intractable. Genetic algorithms (GAs) are population-based stochastic search methods inspired by natural selection that evolve candidate solutions through operations of selection, crossover, and mutation [18]. Genetic algorithms have proven effective for this class of problems [5,6,8] and were therefore employed for park layout optimization [19], combined with K-means clustering [20,21] to identify families of best solutions across multiple independent executions.

3.1. LCOE as Objective Function

To compare scenarios with different cost components, we needed a single metric that integrates capital costs, operational costs, and energy production over the project lifetime. The levelized cost of energy (LCOE) serves this purpose as the standard techno-economic metric for wave energy assessment [22], following the formulation by [21]:

$$LCoE = \frac{CapEx_{y=0} + \sum_{y=1}^{L} \frac{OpEx_y}{(1+r)^y}}{\sum_{y=1}^{L} \frac{AEP_y}{(1+r)^y}} \quad (1)$$

where $CapEx$ is the capital expenditure, $OpEx$ is the operational expenditure, AEP is the annual energy production, L is the project lifetime, and r is the discount rate.

The optimization problem is formally stated as follows:

$$\min_{\{(x_i,y_i)\}_{i=1}^{10}} \quad \mathrm{LCOE}\left((x_i,y_i)_{i=1}^{10}\right) \tag{2}$$

subject to the following constraints:

$$n_{WEC} = 10 \tag{3}$$

$$d_{ij} \geq 3D, \quad \forall\, i \neq j \tag{4}$$

$$(x_i, y_i) \in \Omega, \quad \forall\, i = 1, \ldots, 10 \tag{5}$$

where (x_i, y_i) are the coordinates of the i-th WEC device,

$$(x_c, y_c) = \left(\frac{1}{10} \sum_{i=1}^{10} x_i,\ \frac{1}{10} \sum_{i=1}^{10} y_i \right) \tag{6}$$

(x_c, y_c) is the centroid (arithmetic mean position) of the park, n_{WEC} is the number of wave energy converters, d_{ij} is the Euclidean distance between devices i and j, D is the WEC diameter, and Ω is the computational domain (257 × 257 nodes). The constraint in Equation (4) ensures a minimum spacing of three diameters between devices, based on hydrodynamic interaction studies [19,23]. The centroid serves as the park center from which cable lengths to each device and to the onshore substation are computed.

3.2. Wave Power Calculation

Wave power was computed using the SNL-SWAN spectral wave model [24], a phase-averaged model that solves the spectral action balance equation to propagate wave energy through the domain, accounting for shoaling, refraction, and bottom dissipation. SWAN computes the available wave power directly from the integral of the two-dimensional energy spectrum $E(f, \theta)$:

$$P_{avail} = \rho g \iint c_g(f, d)\, E(f, \theta)\, df\, d\theta \tag{7}$$

where $c_g(f, d)$ is the depth-dependent group velocity, f is frequency, θ is wave direction, and d is water depth. This formulation is valid for arbitrary depth.

Equation (7) is evaluated independently for each of the $N = 179$ representative sea states retained from the 2008–2018 hindcast (see Section 3.3 for the selection procedure), yielding a per-state available wave power field $P_k(x, y)$ for $k = 1, \ldots, N$. The annual mean wave power field used by the optimization is obtained as the weighted sum

$$P_t(x, y) \ = \ \sum_{k=1}^{N} P_k(x, y)\, w_k, \qquad \sum_{k=1}^{N} w_k = 1, \tag{8}$$

where w_k is the annual occurrence probability of sea state k (defined in Section 3.3, Equation (10)). The total park wave power $P_{park} = \sum_{i=1}^{10} P_t(x_i, y_i)$ is the sum of the mean annual wave power at each device location, and the annual energy production is

$$AEP = P_{park}\, H_y\, 10^{-3}, \tag{9}$$

where $H_y = 8514.4$ h is the annual operating time covered by the $N = 179$ retained sea states (97.20% of the 8760 h in a year; see Section 3.3) and 10^{-3} converts watts to kilowatts.

The power assigned to each WEC device in the LCOE calculation is taken to be equal to the available wave power at its grid node, i.e., the device efficiency fraction $\eta = 1$ ($P_{extracted} = P_{avail}$). This implies that each device captures 100% of the incident wave power, a value that is physically unattainable for real WEC devices (typical efficiencies range from 0.1 to 0.4 [25]). The simplification is adopted because the three cost scenarios evaluated in this study all use the same power model: since η enters both the numerator (through CapEx terms proportional to rated power) and the denominator (through AEP) of the LCOE expression, the relative LCOE differences between scenarios are preserved regardless of the assumed efficiency value. The absolute LCOE values reported here are therefore not directly comparable to operational WEC deployments without applying a device-specific efficiency factor. An LCOE sensitivity envelope over realistic η values and the literature interaction-factor range is presented in Appendix A.

3.3. SNL-SWAN Model Configuration

Boundary conditions were derived from the 10-year hindcast (2008–2018) of [15]. A joint H_{m0}–T_p scatter diagram $M_d(H_{m0}, T_p)$ was constructed at a reference boundary node located at the center of the western open boundary, using bins of $\Delta H_{m0} = 0.25$ m (over $H_{m0} \in [0, 5]$ m) and $\Delta T_p = 0.5$ s (over $T_p \in [4, 20]$ s). Bins with annual occurrence $M_d^{(k)} \geq 0.05\%$ were retained, yielding $N = 179$ representative sea states that cover 97.20% of all hindcast observations (8514.4 h out of 8760 h/year). Each retained state k is assigned a weight

$$w_k = \frac{M_d^{(k)}}{\sum_{j=1}^{N} M_d^{(j)}}, \qquad \sum_{k=1}^{N} w_k = 1, \tag{10}$$

which enters the weighted-mean wave power field $P_t(x, y)$ of Equation (8).

For each sea state k and each of the 161 open-boundary nodes, the boundary condition triplet (H_{m0}, T_p, θ) was computed as the temporal mean over all hindcast time steps in which the reference node fell within bin k. Significant wave height and peak period are arithmetic means; mean wave direction is computed as a vector mean to handle wrap-around at 360°. This procedure produces spatially varying JONSWAP spectra along the ∼2.4 km open western boundary rather than a single uniform condition, and is repeated for each of the $N = 179$ retained states. Table 1 summarizes the climatological forcing specifications and the weighted statistics of the resulting catalog.

Table 1. Climatological forcing specifications used to construct the $N = 179$ representative sea states for the SNL-SWAN runs. The retained catalog covers 97.20% of the 2008–2018 hindcast (8514.4 of 8760 h/year); the remaining 2.80% corresponds to bins below the 0.05% occurrence threshold (rare extremes and low-energy outliers) whose contribution to the annual energy budget is negligible. The modal bin (state #38) is listed as a single-state reference; the optimization itself uses the weighted-mean field $P_t(x, y)$ defined in Equation (8).

Climatology source	
Hindcast period	2008–2018 (CFSR-SWAN, [15])
Reference scatter node	center of the western open boundary (offshore)
Scatter diagram	
H_{m0} bin and range	$\Delta H_{m0} = 0.25$ m / $H_{m0} \in [0, 5]$ m
T_p bin and range	$\Delta T_p = 0.5$ s / $T_p \in [4, 20]$ s
Selection threshold	$M_d^{(k)} \geq 0.05\%$

Table 1. *Cont.*

Resulting catalog	
Number of retained states	$N = 179$
Annual time covered	$H_y = 8514.4$ h (97.20% of 8760 h)
Retained range H_{m0}	0.50–3.00 m
Retained range T_p	5.0–18.0 s
Modal bin (state #38)	$H_{m0} = 1.00$ m, $T_p = 13.5$ s, $w = 0.0324$ (276 h/year)
Weighted statistics over the 179 states	
Weighted-mean H_{m0}	1.28 ± 0.39 m (mean $\pm$ weighted std)
Weighted-mean T_p	12.04 ± 2.50 s
Dominant direction	354° N (NNW), annual climatological vector mean
SWAN forcing setup	
Computational domain	$0.4° \times 0.4°$ nested over Bajo San Miguel, BC
Open-boundary nodes	161 (over ∼2.4 km of western boundary)
Spectral shape	JONSWAP

3.4. Cost Scenarios

To isolate the effect of each cost component on the optimization landscape, we use three progressive scenarios summarized in Table 2. Each scenario progressively adds cost components to evaluate their individual and combined effects on optimization results.

Table 2. Experimental scenarios for LCOE calculation.

Scenario	Cable	Depth	Description
CableNoDeepNo	No	No	Base case: energy-based LCOE only
CableSiDeepNo	Yes	No	Adds cable cost to substation
CableSiDeepSi	Yes	Yes	Full model: cable + depth-dependent mooring

By comparing CableNoDeepNo with CableSiDeepNo, we quantify the cable cost effect. Comparing CableSiDeepNo with CableSiDeepSi isolates the bathymetry-dependent mooring effect on LCOE.

The depth-dependent mooring cost follows [12]:

$$Cost_{deep} = Cost_{Mooring} \times 4 \times Depth(x_i, y_i) \tag{11}$$

where $Cost_{Mooring} = 400$ EUR/m [12] is the mooring cost per meter, and $Depth(x_i, y_i)$ is the water depth at each WEC position. The factor of 4 accounts for a typical four-line mooring system. The total mooring cost for the wave park is:

$$C_{WPD} = \sum_{j=1}^{10} Cost_{deep,j} \tag{12}$$

The sensitivity of the LCOE to the mooring cost rate (varied by $\pm 50\%$) and to the discount rate r is reported in Appendix B.

3.5. Genetic Algorithm

The optimization was performed using a binary genetic algorithm adapted from [18]. Each individual is formed by 10 pairs of (x, y) coordinates, each representing the position

of one WEC device within the park. The centroid (arithmetic mean position) of these 10 positions (Equation (6)) is then computed as the wave park center, from which cables extend to each device and to the onshore substation.

The decision to employ a binary genetic algorithm was made due to the discrete nature of the SWAN model grid. A computational grid of 257 × 257 nodes was used, with each device position limited to nodes 3–253 to ensure the complete park remains within the domain. Binary encoding provides a direct mapping to the discrete grid search space: each grid index (range 3–253 in x and y) maps exactly to an 8-bit binary string ($2^8 = 256 > 250$), guaranteeing that every generated individual corresponds to a valid grid position without additional rounding steps [18,26]. Real-coded representations would require discretization to the nearest node after each operation, introducing discretization artifacts and non-smooth fitness landscapes that compromise convergence analysis.

Ten devices were considered for the wave park, with positions optimized by the GA. This number represents a realistic small-to-medium pilot park scale and corresponds to the practical upper limit for classical deterministic optimization methods, enabling potential comparison with boundary element approaches [4]. It is also consistent with park sizes commonly studied in the WEC layout optimization literature [6,19]. The initial position of each device was drawn randomly and independently within the computational domain, allowing the GA to explore the full solution space and converge toward the best park layouts. The minimum spacing between devices was set to three diameters, based on studies by [19,23].

Systematic tests were conducted to identify the best-performing genetic algorithm parameters. Table 3 summarizes the complete experimental design, including all parameter combinations and cost scenarios tested. The mutation rate (p_m) controls the probability of randomly altering each bit in an individual's binary string, governing the balance between exploration and exploitation. The selection probability (p_s) determines the fraction of the population retained as parents for the next generation, controlling selection pressure on the search [18,26].

Table 3. Experimental design: GA parameter combinations and cost scenarios tested. Each of the 48 configurations (16 parameter combinations × 3 scenarios) was executed 100 times, yielding approximately 480 million function evaluations in total.

Component	Values
Genetic Algorithm Parameters	
Mutation rate	0.01, 0.025, 0.05, 0.10 (4 values)
Selection probability	0.6, 0.7, 0.8, 0.9 (4 values)
Population size	100 (fixed)
Maximum iterations	1000 (fixed)
Cost Scenarios	
CableNoDeepNo	Energy-based LCOE only
CableSiDeepNo	LCOE + cable cost to substation
CableSiDeepSi	LCOE + cable + depth-dependent mooring
Experimental Summary	
Parameter combinations	16 (4 mutation × 4 selection)
Cost scenarios	3
Repetitions per configuration	100
Total configurations	48
Total function evaluations	∼480,000,000

3.6. K-Means Clustering Analysis

Genetic algorithms are stochastic and may converge to different solutions across repeated executions [26]. Rather than treating this variability as noise, we used K-means clustering [20,21] to determine whether the GA consistently found families of distinct solutions, providing insight into both the optimization landscape topology and the robustness of results.

The clustering methodology proceeded in four steps:

1. Extraction of the best individual from each of the 100 independent GA executions per configuration;
2. Dimensionality reduction via PCA from 20D (10 WECs $\times$ 2 coordinates) to 2D for visualization;
3. K-means clustering with K ranging from 2 to 10; and
4. Validation using silhouette scores [27] to assess cluster quality.

Four metrics were evaluated for each scenario: optimal K (number of solution families), silhouette score (cluster separation quality, 0–1), diversity (spatial variability in km), and RMS (root mean square distance to centroid, indicating layout compactness).

3.7. Multi-Criteria Selection

This two-level selection procedure (a composite score for the configuration and the K-means cluster centroid for the layout) was adopted because the absolute best layout, while achieving the lowest cost, represents a single outcome from one specific GA execution and is therefore sensitive to the random initialization of that run. The *star-layout*, by contrast, captures the spatial structure that the GA recovers consistently across multiple executions; it is more representative of the underlying optimization landscape and is therefore preferred for practical interpretation.

Within each cost scenario, the 16 GA parameter combinations (4 mutation rates $\times$ 4 selection probabilities) are ranked by a composite score that balances five performance metrics computed across the 100 independent executions of each combination:

- The absolute minimum cost achieved (best_cost, lower is better);
- The median cost across executions (median_cost, lower is better, measures typical performance);
- The 10th-percentile cost (p10_cost, lower is better, measures bottom-decile run quality);
- The coefficient of variation of the cost distribution (cv_cost = std_cost/mean_cost, lower is better, measures consistency between runs);
- The percentage of executions with cost within 5% of the absolute minimum (pct_within_5pct, higher is better).

Each metric is min–max normalized across the 16 combinations of the same scenario (the lowest value in each scenario maps to 0, the highest to 1); the percentage metric is inverted ($1 - \tilde{p}$) so that lower values uniformly indicate better performance for all five terms. The composite score is then the weighted sum

$$S = 0.40\,\tilde{c}_{\text{best}} + 0.30\,\tilde{c}_{\text{med}} + 0.15\,\tilde{c}_{\text{p10}} + 0.10\,\tilde{c}_{\text{cv}} + 0.05\,(1 - \tilde{p}_{5\%}), \tag{13}$$

where the tilde denotes the min–max normalized value of each metric. The weights prioritize the achieved minimum cost (0.40) and the typical-run performance (0.30), with smaller contributions from the bottom-decile quality, the run-to-run consistency, and the percentage of competitive solutions. The combination with the smallest S in each scenario is selected as the rank-1 (*star*) configuration. This multi-criteria approach aligns with recent developments in WEC park optimization that recognize the need to balance competing objectives [7].

Once the rank-1 configuration is selected, the K-means clustering described in Section 4.3 is applied to the 100 best-of-execution layouts of that configuration. The dominant cluster (the largest by membership) defines the *star-layout*: each of its 10 WEC positions is the arithmetic mean of the corresponding WEC positions across all layouts in the dominant cluster. The *star-layout* is used as the representative layout of the scenario throughout the manuscript, alongside the absolute best layout (the single layout achieving best_cost) for the comparisons of Section 4.

4. Results

The optimization framework described above was applied to Todos Santos Bay under three different scenarios, with 100 independent GA executions per parameter combination. The results are organized as follows: we first present GA parameter calibration and convergence analysis, then characterize solution families through K-means clustering and variability ellipses, then present the proposed layouts derived from that clustering analysis, and finally quantify the effects of each cost component through scenario comparison.

4.1. GA Parameter Calibration

The systematic parameter study revealed that higher mutation rates (0.05–0.10) consistently outperformed lower rates across all scenarios, suggesting that the bathymetry-influenced landscape in this study benefits from increased exploration capacity [28,29]. Table 4 reports the rank-1 (mutation, selection) combination of each scenario, selected by the multi-criteria composite score of Section 3.7 (Equation (13)), together with the *star-layout* LCOE and three inter-run cluster diagnostics: the number of K-means clusters K, the silhouette score, and the layout RMS (mean per-WEC displacement between best-of-execution layouts). All three diagnostics improve monotonically as cost components are added: K decreases ($4 \rightarrow 3 \rightarrow 2$), the silhouette score increases ($0.627 \rightarrow 0.709 \rightarrow 0.855$), and the layout RMS shrinks by $\sim$65% ($2106 \rightarrow 1482 \rightarrow 741$ m), confirming that each cost component progressively narrows the optimization landscape and increases the reproducibility of the GA across independent executions.

Table 4. GA parameter combinations selected by the multi-criteria analysis for each cost scenario (see Section 3.7), with the LCOE of the representative *star-layout* (centroid of the dominant cluster) and inter-run cluster diagnostics: number of K-means clusters K, silhouette score, and layout RMS. The layout RMS is the mean per-WEC RMS displacement between any two best-of-execution layouts of the rank-1 configuration (lower values indicate more reproducible GA results across executions); it is obtained from the mean pairwise distance in 20-dimensional node space ($\langle d_{ij} \rangle$) as $\langle d_{ij} \rangle / \sqrt{10}$, scaled by the geometric mean of the node resolutions ($\sqrt{36.7 \times 43.4} \simeq 39.9$ m/node). LCOE is computed on the *star-layout* coordinates via the cost model of Section 3.1; values are in EUR/MWh.

Scenario	Mut.	Sel.	LCOE (EUR/MWh)	Silhouette	K	Layout RMS (m)
CableNoDeepNo	0.10	0.7	153.36	0.627	4	2106
CableSiDeepNo	0.05	0.8	233.38	0.709	3	1482
CableSiDeepSi	0.10	0.6	270.81	0.855	2	741

The table shows that a mutation rate of 0.10 yielded the best multi-criteria score in 2 of 3 scenarios. Silhouette scores range from 0.627 (CableNoDeepNo, K = 4) to 0.855 (CableSiDeepSi, K = 2), indicating well-defined solution families in each case. Notably, the number of clusters decreases monotonically as cost components are added ($K = 4 \rightarrow 3 \rightarrow 2$), reinforcing that infrastructure constraints progressively reduce the viable solution space.

4.2. GA Convergence Analysis

The genetic algorithm's stochastic nature produces variability across executions, making statistical analysis essential. Each scenario comprised 100 independent executions with random initialization, and statistics were computed with the best individual from each execution following [30]. This approach assumes that WEC park design is an optimization problem where only the best achievable result matters for practical implementation.

Figure 4 shows histograms of device positions at algorithm termination (iteration 1000) for the best-performing mutation and selection combinations in each scenario. The background colors and contours represent wave power distribution (kW/m) across the study domain; the complete color scale is shown in Figure 2. The same color scale applies to all spatial maps in this section.

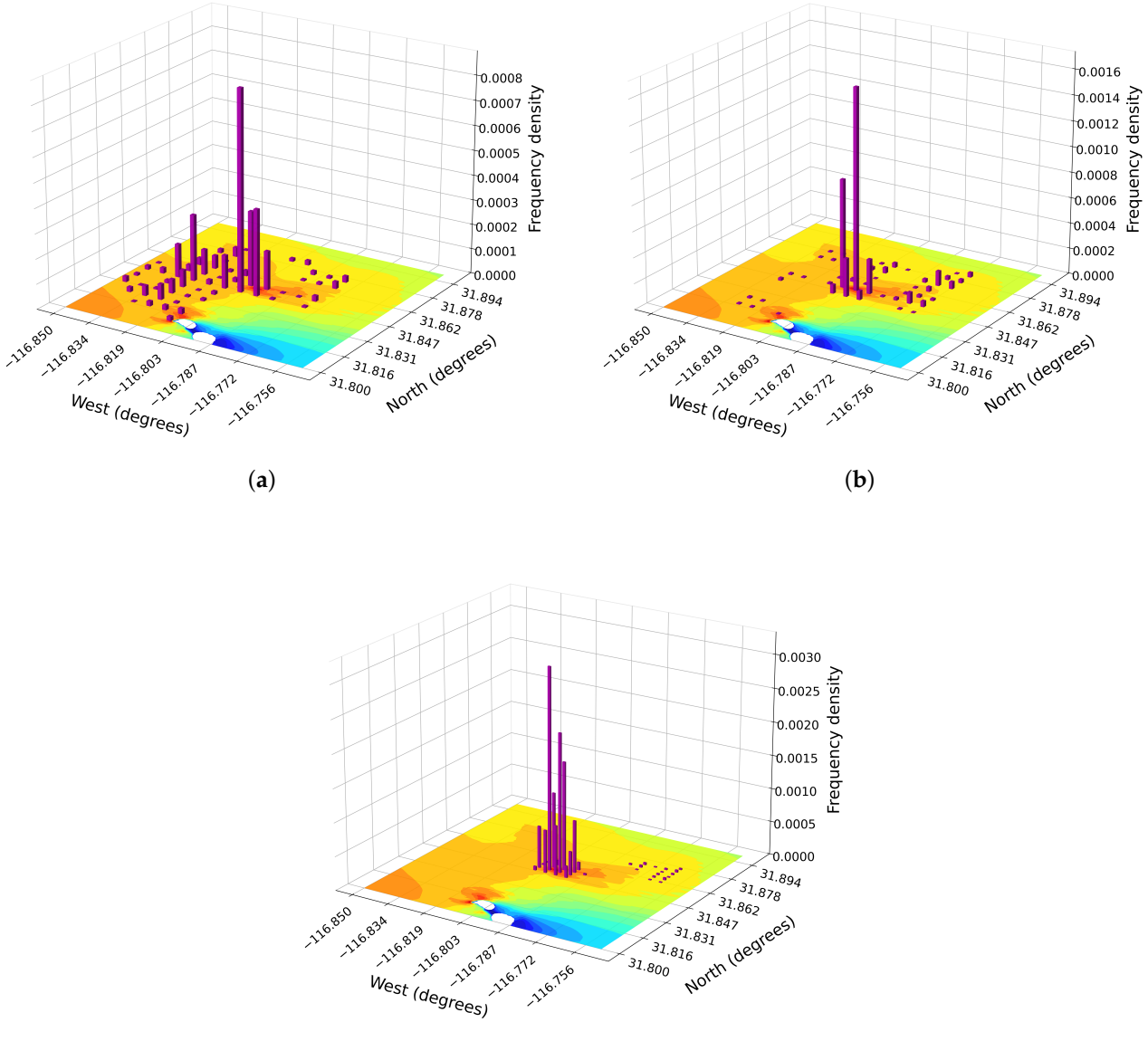

Figure 4. 3D histograms of solution distribution across the park domain for the three cost scenarios. Each bar represents the frequency of WEC layouts within a spatial bin, illustrating the spatial concentration of converged solutions. All three panels use the same z-axis (layout frequency) color scale to allow direct visual comparison across scenarios. The contour at the base of each panel is the positive wave-power density field $P_t(x, y)$ (kW/m), weighted over the 179 sea states of the 2008–2018 climatology (Equation (8)); (**a**) CableNoDeepNo, (**b**) CableSiDeepNo, (**c**) CableSiDeepSi.

In the CableNoDeepNo scenario (Figure 4a), wave power dominates the optimization landscape. Devices concentrate near San Miguel Reef, the primary wave-focusing feature in the study region, even without cable cost penalties. A secondary cluster appears between latitudes [31.800°, 31.801° N] and longitudes [−116.849°, −116.850° W], where high power coincides with sufficient space to satisfy inter-device spacing constraints. Clustering analysis of the 100 independent runs confirms this bimodal distribution: 60% of solutions converge to the primary cluster near San Miguel Reef, with the remaining 40% distributed across secondary locations.

Including cable costs (CableSiDeepNo, Figure 4b) increases device concentration near San Miguel Reef while reducing outliers in distant locations. This shift reflects the trade-off between wave power maximization and cable length minimization imposed by grid connection requirements. Clustering analysis quantifies this consolidation: 82% of the 100 runs converge to the dominant cluster (up from 60% in CableNoDeepNo), directly measuring the reduction in solution diversity imposed by cable cost constraints.

The full cost scenario (CableSiDeepSi, Figure 4c) shows substantially tighter clustering than CableSiDeepNo, with fewer devices in deeper zones. The dominant cluster reaches 97% of solutions, a 15-percentage-point increase over CableSiDeepNo, and the K-means partition simplifies from K = 3 to K = 2 (silhouette 0.709 $\rightarrow$ 0.855; see Table 4). This sharpening is consistent with the +16.0% LCOE contribution of the bathymetry-dependent mooring cost: the additional depth-dependent cost gradient eliminates the marginally viable layouts that were still tolerated under cable-only optimization, leaving a single dominant solution family plus a small group of outlier runs with substantially higher cost.

Figure 5 presents the best LCOE achieved across all mutation and selection rate combinations for each scenario. From the 100 independent executions per configuration, the absolute best result is shown.

For the CableNoDeepNo scenario (Figure 5a), the best result is obtained with mutation = 0.10 and selection = 0.7 (151.42 EUR/MWh). A gradient of improved solutions emerges as the mutation rate increases, confirming that higher exploration capacity benefits this multimodal landscape.

The CableSiDeepNo scenario (Figure 5b) shows the absolute minimum at mutation = 0.05 and selection = 0.7 (229.03 EUR/MWh). The LCOE values are approximately 80 EUR/MWh higher than in CableNoDeepNo due to the cable cost (a +51% increase); higher mutation rates (0.05–0.10) consistently outperform lower rates across the heatmap.

In the full cost scenario, CableSiDeepSi (Figure 5c), the best-performing values shift to mutation = 0.025 and selection = 0.9 (265.29 EUR/MWh). The LCOE values are approximately 36 EUR/MWh higher than in CableSiDeepNo due to bathymetry-dependent mooring costs, a further +16% increase that complements the larger cable-cost effect; cable costs remain the larger of the two infrastructure cost components, but bathymetry-dependent mooring is also material.

Convergence analysis revealed a clear trade-off between exploration and exploitation. Lower mutation rates produced fast but premature convergence to suboptimal final costs; higher mutation rates delayed convergence but consistently achieved better global optima. This pattern differs from typical GA applications, where mutation rates of 0.01–0.02 are standard, and is consistent with the expected behavior in multimodal optimization landscapes [21,28,29,31].

Figure 6 shows the convergence envelope of the rank-1 GA configuration in each scenario. The mean trajectory reaches within 5% of its final value by iteration ∼70 in all three scenarios; the run-to-run variability ($1\sigma \approx$ 12–15 EUR/MWh) persists at convergence and reflects the inherent stochasticity of the GA initialization. This statistical

envelope complements single-execution convergence curves shown later in this section for each scenario.

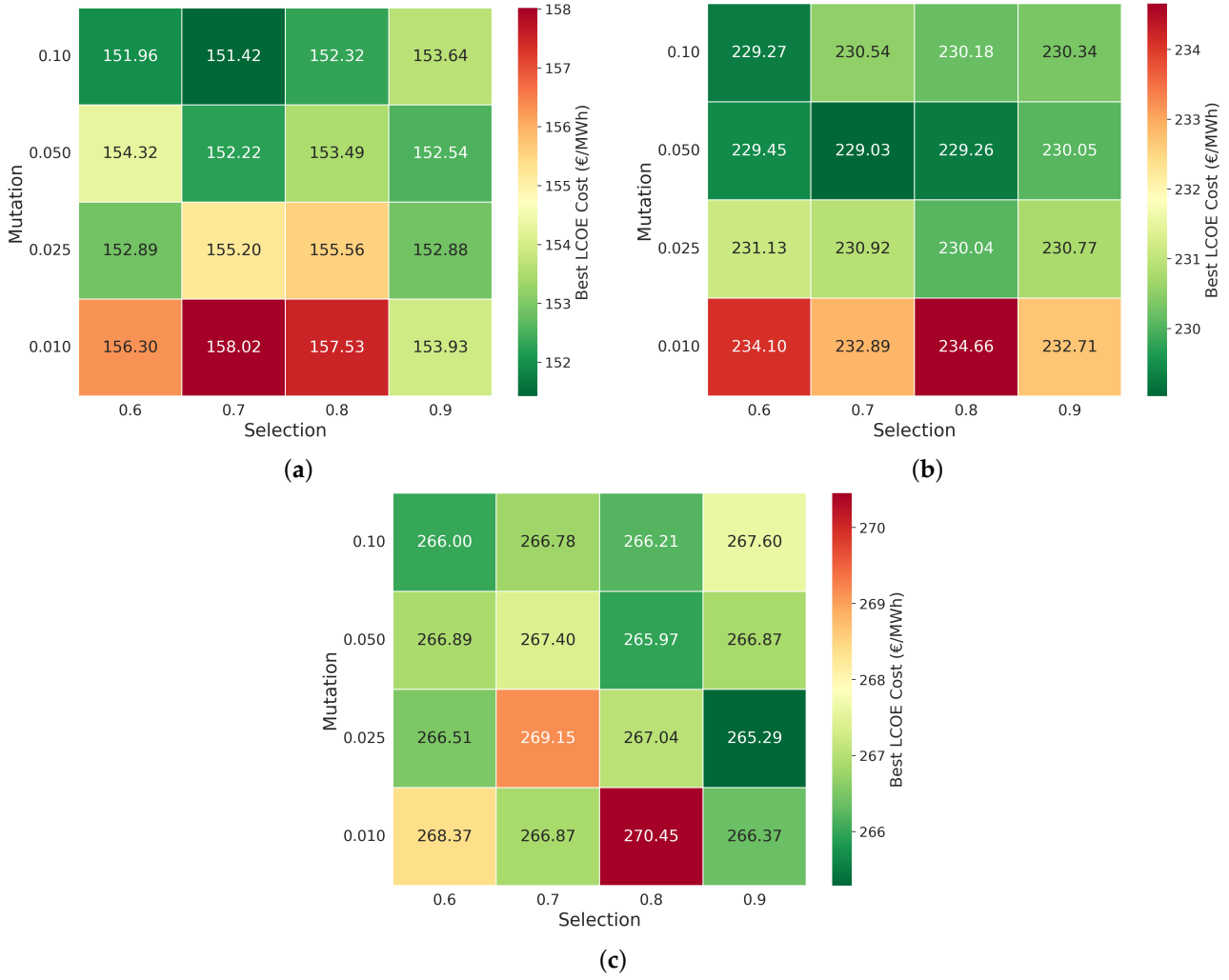

Figure 5. Best LCOE achieved across combinations of mutation and selection rates for the three cost scenarios. Darker colors indicate lower (better) LCOE values. All three panels use the same colormap convention; each panel's color range spans the LCOE values of its own scenario, so visual comparison is meaningful within a panel, and the absolute values printed in each cell should be used for cross-panel comparison; (**a**) CableNoDeepNo, (**b**) CableSiDeepNo, (**c**) CableSiDeepSi.

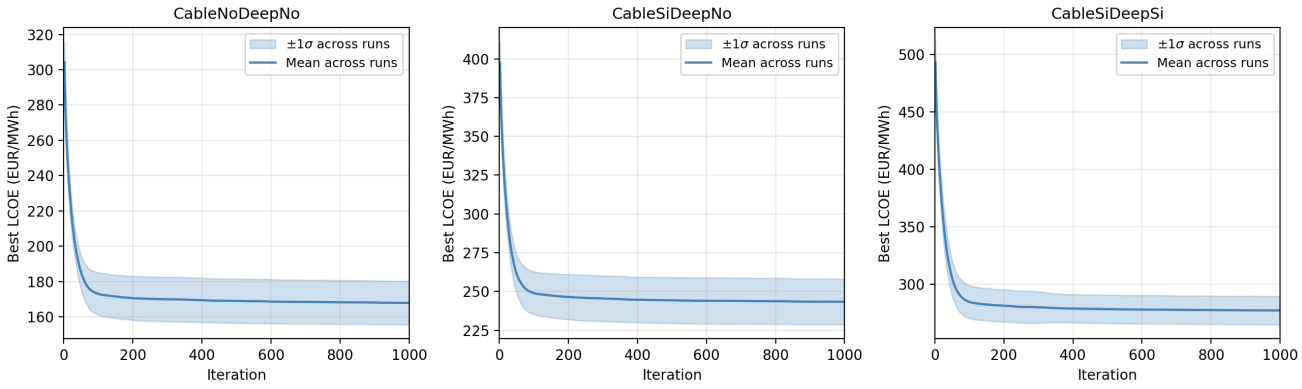

Figure 6. Convergence envelopes for the rank-1 GA configuration of each cost scenario. Solid line: mean across the 100 independent executions; shaded band: $\pm 1\sigma$.

4.3. K-Means Clustering and Variability Ellipses

The histogram analysis provides a preliminary overview, but quantifying solution variability requires additional tools. Variability ellipses (Figures 7–9, left panels) characterize the spatial distribution of best solutions found across executions. Each panel displays two confidence regions: one standard deviation (68% of solutions) and two standard deviations (95% of solutions). The elongated ellipse shapes follow the wave power distribution shown as background colors in the left panels, confirming that the GA explores solutions along the dominant energy gradient. Yellow diamonds indicate the layout with the highest reproducibility.

The right panels of Figures 7–9 present K-means clustering results. These plots project the 10-device park layouts onto a two-dimensional space defined by the first two principal components (PC1 and PC2), which together capture approximately 90% of the total variance. In this space, each point represents a WEC park layout; closer points indicate more similar layouts. The silhouette scores reported in the right panels (0.627 for CableNoDeepNo, 0.709 for CableSiDeepNo, 0.855 for CableSiDeepSi; see Table 4) indicate progressively more sharply defined solution families as cost components are added.

A noteworthy finding from this clustering analysis is the size of the dominant cluster in each scenario. In Figure 7, the primary cluster contains 60 parks (out of 100); in Figure 8, it contains 82 parks; and in Figure 9, it contains 97 parks. The latter case is particularly striking: 97 of 100 optimized parks exhibit layouts highly similar to the *star-layout*, with only 3 outlier runs converging elsewhere, indicating strong convergence and reproducibility of the optimization under the full cost model.

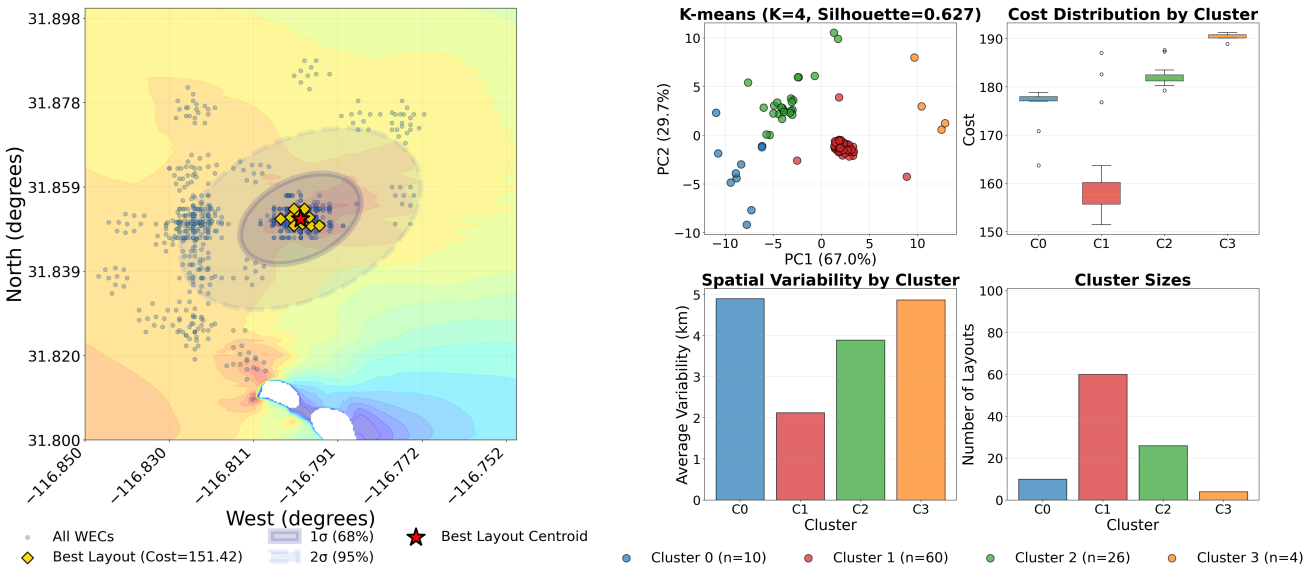

Figure 7. Clustering analysis for the CableNoDeepNo scenario. (**Left**): Variability ellipse showing the spatial distribution of WEC positions across 100 GA executions overlaid on the positive wave-power density field $P_t(x, y)$ (color scale, kW/m), weighted over the 179 sea states of the 2008–2018 climatology (Equation (8)); the red star indicates the proposed layout centroid, solid ellipse shows 1σ (68%) confidence region, dashed ellipse shows 2σ (95%) region. (**Right**): K-means analysis showing PCA projection of solution families, cost distribution, spatial variability, and cluster sizes. The wave-power background color scale is shared across Figures 7–9, so the wave-energy field is visually comparable across the three scenarios.

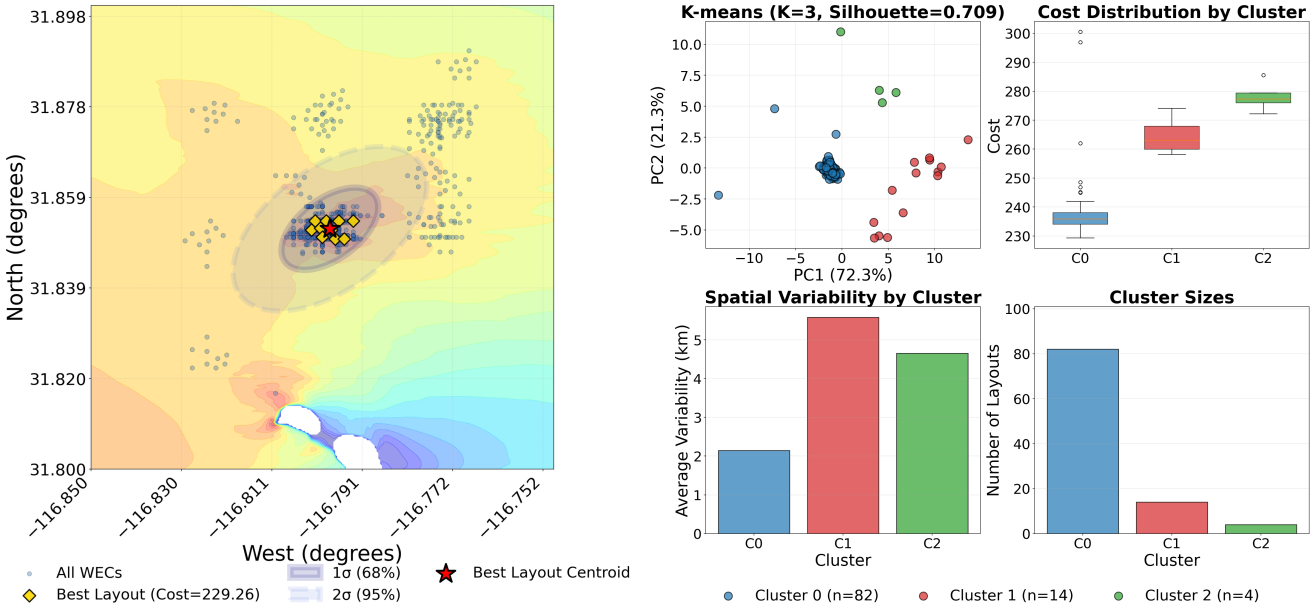

Figure 8. Same as Figure 7 but for the CableSiDeepNo scenario (with cable costs). (**Left**): the variability ellipse is more elongated than in Figure 7, and a substantial fraction of WEC positions has shifted to the eastern half of the domain (approximately [−116.811°, −116.850° W]), reducing the cable length to the SE Sauzal substation; including the cable term in the objective raises the absolute LCOE, but the optimization compensates by relocating the park closer to shore. (**Right**): the dominant family (cluster 0, 82 of 100 executions) is compact and consistent with the tight 1σ contour in the left panel. The cluster index of the dominant family changes from 1 in Figure 7 to 0 here because *k*-means cluster IDs are arbitrary labels assigned at each (re-)initialization and carry no semantic meaning across scenarios.

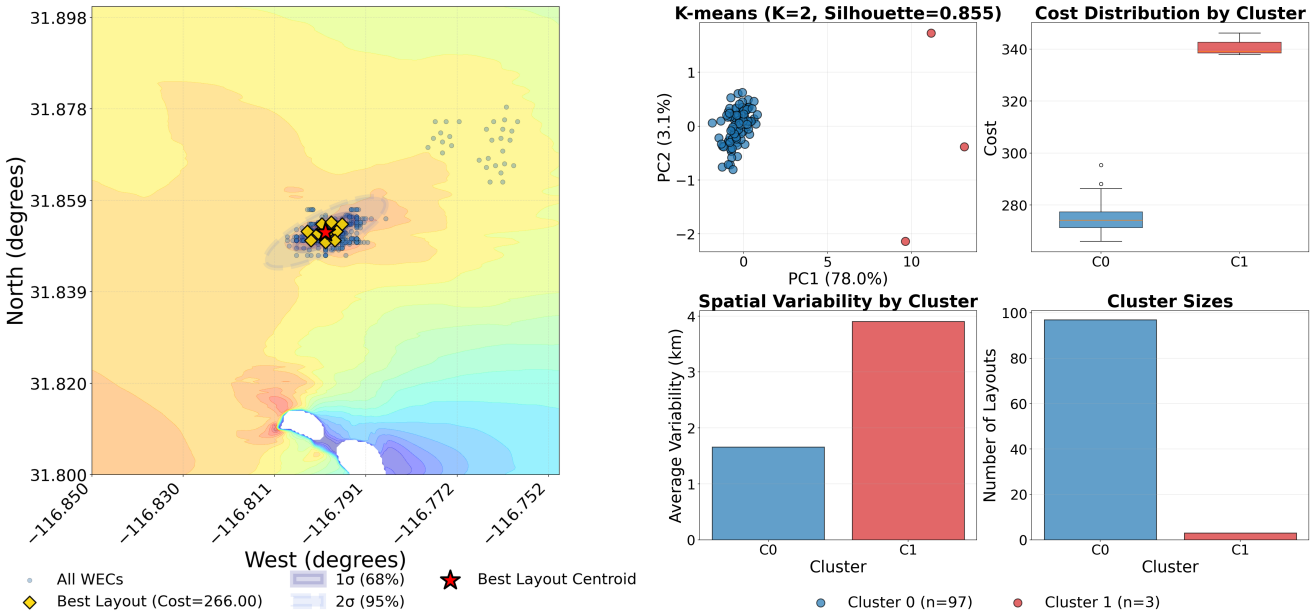

Figure 9. The same as Figure 7 but for the CableSiDeepSi scenario (cable and depth costs). (**Left**): both variability ellipses are considerably smaller than in the two previous scenarios and more strongly elongated, reflecting the combined penalty of cable and bathymetry-dependent mooring costs. The WEC positions concentrate near San Miguel Reef, where the wave-focusing maximum coincides with locally shallower water that reduces the mooring contribution. (**Right**): 97 of 100 executions fall in the dominant cluster (cluster 0), indicating that the additional cost gradient drives the GA toward a single, highly reproducible layout.

The clustering analysis reveals how the number of distinct solution families changes across cost scenarios. Figures 7–9 present the variability ellipses and cluster analysis for each scenario. The inclusion of cable costs (Figure 8) reduces the number of solution families from K = 4 to K = 3, indicating that grid connection requirements constrain the feasible solution space; the smaller variability ellipse compared to Figure 7 reflects the stronger convergence when cable costs are included. Adding the bathymetry-dependent mooring cost (Figure 9) further reduces the partition to K = 2 one dominant solution family of 97 parks plus a small group of 3 outlier runs with substantially higher cost and increases the silhouette score from 0.709 to 0.855 (Table 4). This monotonic sharpening ($K = 4 \rightarrow 3 \rightarrow 2$) confirms that each cost component progressively narrows the optimization landscape, with bathymetry-dependent mooring adding a nontrivial second sharpening step.

The clustering results show that solution families become more concentrated as cost components are added, with the variability ellipses decreasing in size. The transition from K = 4 to K = 3 clusters when cable costs are included represents a 25% reduction in solution diversity, demonstrating that grid connection requirements constrain the feasible solution space. In particular, the solution cluster located near 31.83° N and −116.845° W in the CableNoDeepNo scenario (Figure 7) disappears as cost components are added: its western position maximizes the cable run to the SE Sauzal substation, so it is already absent once cable costs are included (Figure 8), and the surviving solutions then consolidate near San Miguel Reef when the bathymetry-dependent mooring cost rewards the shallower water there (Figure 9).

4.4. Proposed Layout Analysis

Figures 10–12 present the proposed layouts identified through the multi-criteria clustering analysis described above (Section 4.3), showing layouts that balance minimum cost, robustness, and reproducibility rather than the absolute minimum LCOE alone. Each figure displays the GA convergence trajectory (upper panels) and the spatial layout overlaid on wave power contours (lower panel), with blue dots indicating initial positions and magenta dots showing final device locations.

The selected layouts are statistically robust solutions to which the GA converges consistently across multiple executions. Although their LCOE differs from the absolute heatmap minimum by approximately 2–6 EUR/MWh (∼1–2%, depending on the scenario), they provide greater confidence for practical deployment decisions. Notably, all three scenarios show convergence toward San Miguel Reef, but with progressively tighter clustering as cost components are added, a pattern already quantified in the clustering analysis above.

In the CableNoDeepNo scenario (Figure 10), the proposed layout (153.36 EUR/MWh) is positioned over San Miguel Reef, the secondary wave power maximum, demonstrating a preference for the accessible high-energy zone. The inclusion of cable cost in CableSiDeepNo (Figure 11) shifts the proposed layout closer to the substation while maintaining proximity to the wave energy concentration (233.38 EUR/MWh, +52.2% over the no-cable scenario; see Table 5). The full cost scenario CableSiDeepSi (Figure 12) further constrains the optimization, balancing wave power, cable distance, and water depth (270.81 EUR/MWh, +16.0% over the cable-only scenario; see Table 6); the bathymetry-dependent mooring contribution is the smaller of the two infrastructure cost components but is far from negligible, and produces a 151 m park-center reorganization relative to CableSiDeepNo (Table 6).

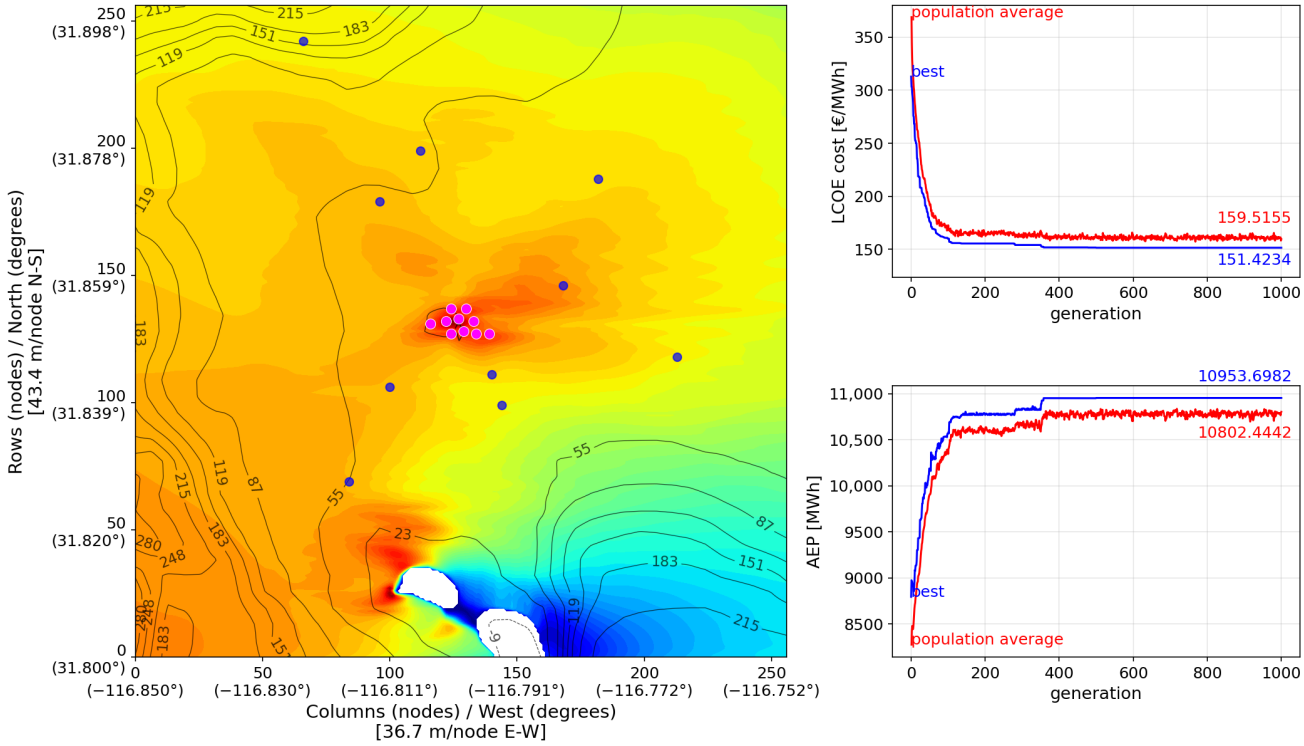

Figure 10. Proposed park layout for the CableNoDeepNo scenario (no cable or depth costs). (**Left**): WEC positions overlaid on the wave power field (color scale, kW/m); black contours indicate bathymetry. Blue dots indicate initial random WEC positions; magenta dots show the final positions after 1000 generations. (**Right**): LCOE (**top**) and AEP (**bottom**) convergence curves.

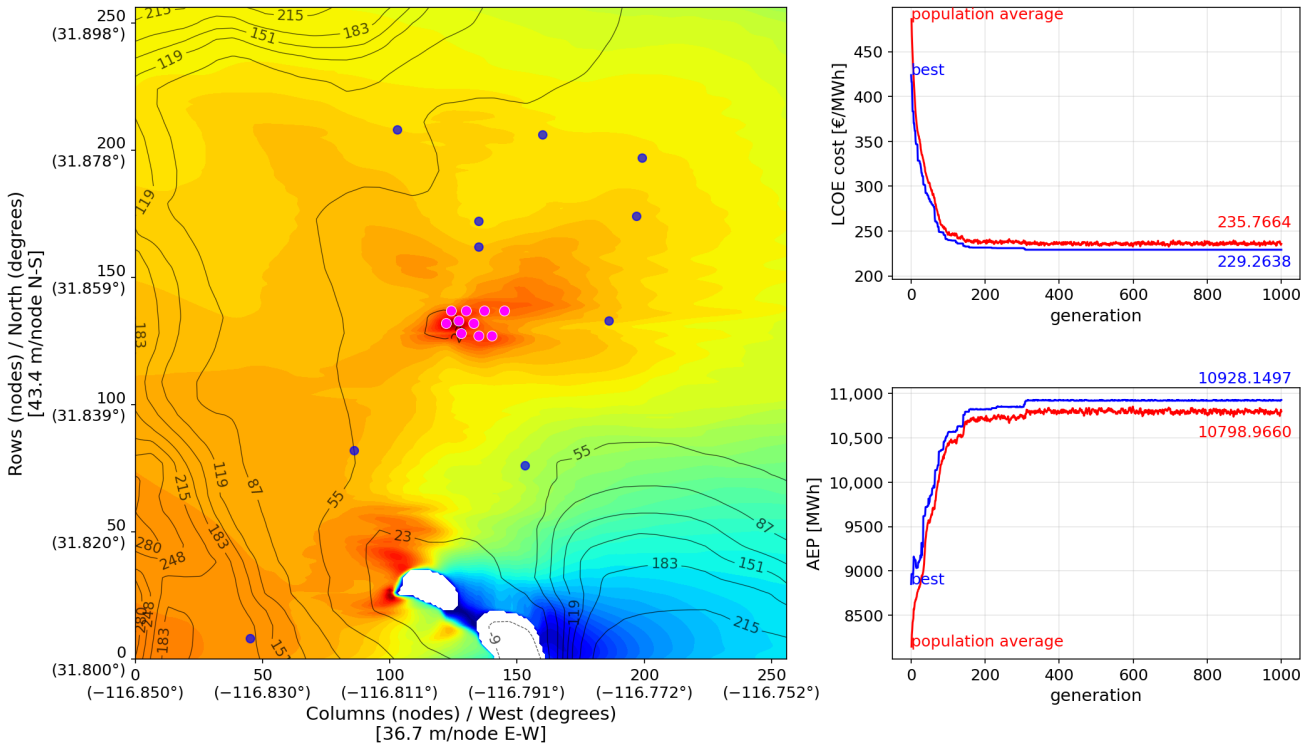

Figure 11. Same as Figure 10 but for the CableSiDeepNo scenario (with cable costs).

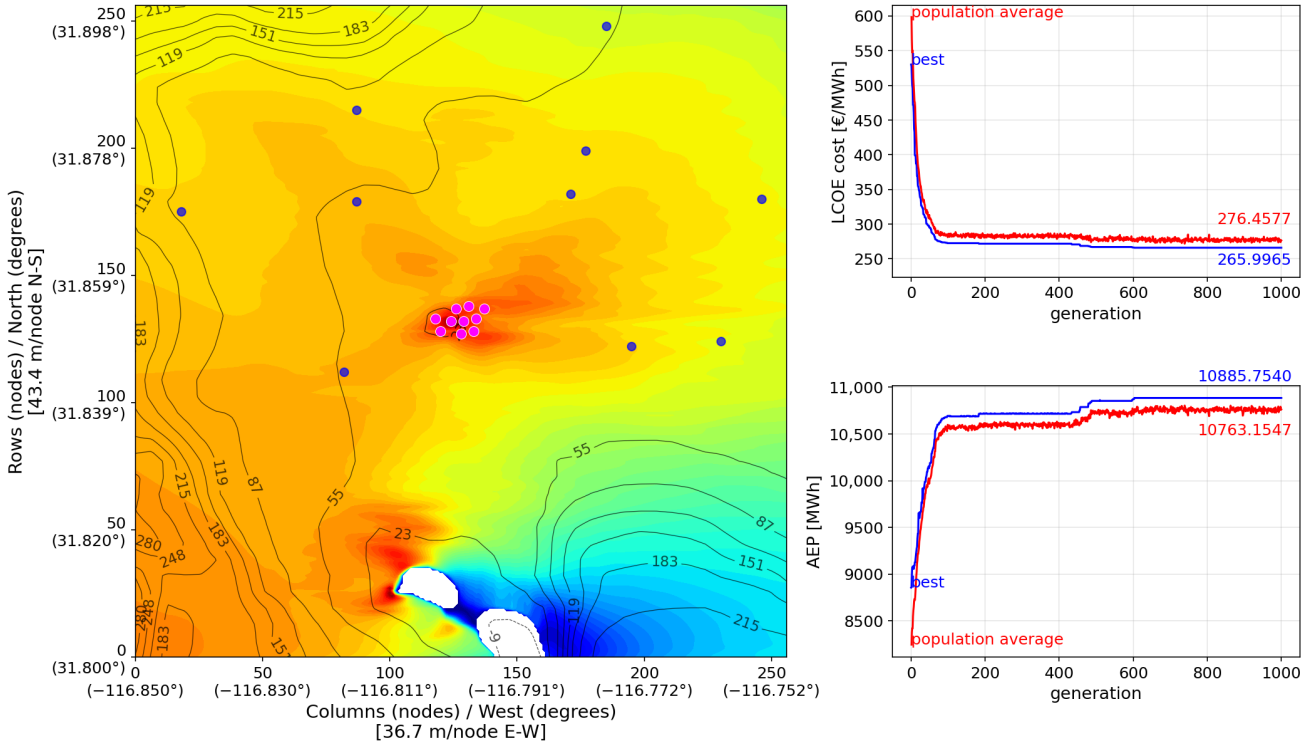

Figure 12. Same as Figure 10 but for the CableSiDeepSi scenario (cable and depth costs).

4.5. Scenario Comparison

Figure 13 illustrates two complementary approaches for interpreting genetic algorithm results in WEC park optimization. The first row displays the absolute minimum LCOE layouts for each scenario (Figure 5a–c). These solutions exhibit predominantly linear or aligned arrangements, consistent with findings reported in the comprehensive review by [3], who noted that linear layouts frequently emerge as optimal in WEC park optimization studies.

The second row presents an alternative approach based on K-means clustering analysis (Section 4.3). These proposed layouts, hereinafter referred to as *star-layouts*, correspond to those identified from the mutation and selection operator combinations that yield the most consistent and reproducible results. Unlike the absolute minima, the K-means-derived solutions follow more closely the spatial distribution of the wave power resource, adapting to the natural shape of the high-energy zones. This approach offers a significant practical advantage: the genetic algorithm demonstrates better overall performance with these operator combinations, producing solutions that are more likely to be replicated across independent executions.

Both the absolute best-found and *star-layouts* achieve similar LCOE values, with differences below 2% across all scenarios (CableNoDeepNo: 151.42 vs. 153.36 EUR/MWh; CableSiDeepNo: 229.03 vs. 233.38 EUR/MWh; CableSiDeepSi: 265.29 vs. 270.81 EUR/MWh); however, the absolute optima obtained with different operator combinations have a lower probability of occurrence, making them less reliable from a practical standpoint.

In the scenario without cable or bathymetry-dependent mooring costs (first column of Figure 13), the park exhibits proportional dimensions along both the x and y axes. In contrast, the scenario with cable cost but without bathymetry-dependent mooring (second column) shows a more elongated layout along the x-axis than the y-axis, following the spatial distribution of wave power in this zone. In the third scenario, which includes both cable and bathymetry-dependent mooring costs, the park layout adjusts to optimize the maximum power zone. It should be noted that wave power in this study is directly affected by bathymetry, even when bathymetry is not explicitly considered in the cost function.

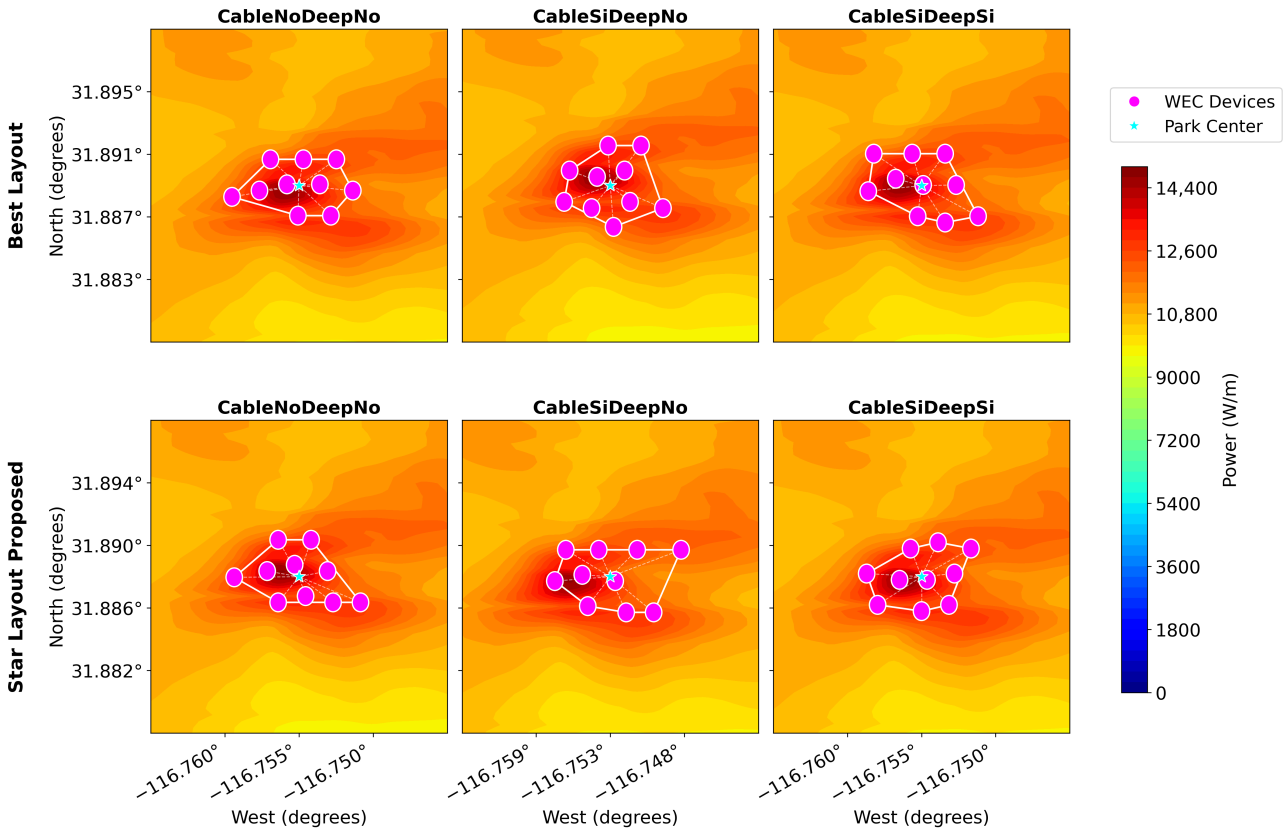

Figure 13. Comparison of the best layout ((**top**) row) vs. the proposed *star-layout* ((**bottom**) row) for the three cost scenarios: CableNoDeepNo, CableSiDeepNo, and CableSiDeepSi ((**left**), (**center**), and (**right**) columns, respectively). The top row shows the layouts with the lowest absolute cost; the bottom row shows the representative *star-layouts* from clustering analysis. The best layout consistently achieves lower costs than the *star-layout* across all scenarios.

Cable costs emerged as the dominant factor in the optimization. Table 5 summarizes the comparison between scenarios without and with cable costs.

The 52.2% LCOE increase is accompanied by a 172 m spatial shift of the park center, dominated by the east–west component (+158 m) with a smaller north–south component (+70 m). This shift is comparable to the typical inter-WEC spacing in the optimized layouts and indicates that cable cost rebalances the trade-off between proximity to the wave-energy concentration and proximity to the shore connection point. The optimization does not, however, abandon the dominant wave-focusing region, confirming that wave-energy availability remains a primary driver even when grid-connection costs are imposed.

Table 5. Effect of submarine cable cost on the *star-layout* LCOE and cluster structure (CableNoDeepNo vs. CableSiDeepNo). Park-center coordinates are the centroid (arithmetic mean) of the dominant cluster's WEC positions.

Metric	CableNoDeepNo	CableSiDeepNo	Change
LCOE (EUR/MWh)	153.36	233.38	+52.2%
Silhouette	0.627	0.709	+13.1%
K clusters	4	3	−1
Park Center E–W (km)	4.693	4.851	+158 m
Park Center N–S (km)	5.684	5.754	+70 m
Total displacement			172 m

In stark contrast to cable costs, bathymetry-dependent mooring had a marginal effect in this study area. Table 6 summarizes the comparison when depth-dependent costs are added.

Adding the bathymetry-dependent mooring cost produces a further 16.0% increase in LCOE and a 151 m spatial shift of the park center, predominantly in the east–west direction (the north–south displacement is only −9 m). The K-means cluster structure simplifies from K = 3 to K = 2 (silhouette score rises from 0.709 to 0.855), indicating that the additional cost constraint sharpens the optimal solution family into a single dominant cluster plus a small group of outlier runs. The relative magnitudes of the cable and mooring contributions are discussed in Section 5.

Table 6. Effect of bathymetry-dependent mooring cost on the *star-layout* LCOE and cluster structure (CableSiDeepNo vs. CableSiDeepSi). Park-center coordinates are the centroid (arithmetic mean) of the dominant cluster's WEC positions.

Metric	CableSiDeepNo	CableSiDeepSi	Change
LCOE (EUR/MWh)	233.38	270.81	+16.0%
Silhouette	0.709	0.855	+20.6%
K clusters	3	2	−1
Park Center E–W (km)	4.851	4.700	−150 m
Park Center N–S (km)	5.754	5.745	−9 m
Total displacement			151 m

5. Discussion

The results presented above reveal a clear hierarchy among cost components in WEC park optimization: including cable costs raised LCOE by 52.2%, while adding bathymetry-dependent mooring costs raised it by a further 16.0%, a ratio of approximately 3:1 in terms of LCOE sensitivity between these two cost components. Both contributions are nontrivial, supporting the central hypothesis of this work that bathymetry-dependent costs cannot be safely neglected at sites with nontrivial depth variation.

5.1. Interpretation of Cost Component Effects

Submarine cable costs represent the larger of the two infrastructure cost contributions. The +52.2% increase in LCOE between the CableNoDeepNo and CableSiDeepNo scenarios (Table 5) demonstrates that ignoring cable costs leads to a substantial underestimation of project costs. This cost increase is accompanied by a 172 m spatial shift of the park center, predominantly in the east–west direction, which rebalances the trade-off between proximity to the wave-energy concentration and proximity to the shore connection point without abandoning the dominant wave-focusing region.

The relative magnitude of the two contributions can be understood through the cost structure. The cable contribution combines a fixed cost proportional to the absolute distance from the park centroid to the shore connection (export cable at 72.5 EUR/m, plus intra-park collection at 46 EUR/m) with the spatial gradient that this distance creates across the optimization domain. The bathymetry-dependent mooring cost (Equation (11)) yields a gradient of 1600 EUR per meter of depth increase (400 EUR/m × 4 lines per device). Given the depth range in the study domain (20–40 m), the maximum mooring cost variation is approximately 32,000 EUR per device, or 320,000 EUR for a 10-device park. The 172 m and 151 m spatial displacements (Tables 5 and 6) confirm that both cost components create spatial gradients sufficient to influence the proposed layouts within the dominant wave-focusing region, rather than redirecting the optimization to a different region of the domain.

This cost hierarchy reflects actual economic magnitudes rather than a scale artifact of the chosen units. Both components are expressed in the same monetary units (EUR) and enter the LCOE objective additively, making the relative LCOE sensitivities (+52.2% vs. +16.0%) a dimensionless, naturally normalized comparison. The convergence of all scenarios to layouts that remain within the dominant wave-focusing region, while shifting by 150–170 m in response to each cost component, confirms that infrastructure costs at this site act as fine-tuning forces on top of the wave-power landscape rather than as gross redirection forces.

Bathymetry-dependent mooring costs add a 16.0% increase in LCOE on top of the cable-only baseline. Although smaller than the cable contribution, this is a substantial fraction of the LCOE budget that flat-bathymetry analyses systematically miss. The 151 m spatial reorganization driven by adding mooring, predominantly in the east–west direction, is consistent with the depth gradient of the optimization domain (20–40 m range): the optimization repositions the park to 'compromise' wave-power capture for shallower water, demonstrating that the mooring cost function does carry sufficient spatial discrimination to influence the proposed park positions when superimposed on the wave-power and cable-cost landscape.

Having established the mechanistic basis for the relative magnitudes of both infrastructure cost components, we now contextualize these findings within the broader WEC optimization literature.

5.2. Comparison with Literature

5.2.1. Cost Component Hierarchy

Previous WEC park optimization studies predominantly assumed flat bathymetry and often omitted cable costs entirely [3,5]. This study demonstrates that omitting cable cost alone underestimates LCOE by 52.2%, and that further omitting bathymetry-dependent mooring underestimates it by an additional 16.0%, for a combined underestimation of more than 70% of the no-infrastructure baseline. Both simplifications are routinely made in the literature; our results indicate that neither is benign at sites with nontrivial depth variation, with direct implications for project cost assessment in early planning stages.

Our results agree with the findings of [9], who demonstrated that the financial parameters (specifically the discount rate) dominated the optimization of hybrid wind-wave farms over physical site characteristics. Similarly, we find that infrastructure costs exert a strong influence on the optimization. Our work extends this understanding by quantifying the relative magnitude of the two infrastructure cost components included here: cable effects are approximately three times larger than bathymetry-dependent mooring effects in terms of LCOE impact (+52.2% vs. +16.0%), with both contributions material rather than one being a dominant gradient and the other negligible.

This cost hierarchy has implications for the broader marine renewable energy literature. Ref. [11] identified bathymetry as critical for site selection, but their analysis focused on feasibility constraints (minimum depth, seabed conditions) rather than optimization gradients within feasible zones. Our results show that within feasible areas, bathymetric variation has a material influence on the proposed layouts even at the moderate depth gradients of Todos Santos Bay. For sites with steeper gradients, or for floating WEC technologies where mooring costs scale more strongly with depth [12], this contribution can be expected to be even larger.

5.2.2. Park Layouts

The best layouts found (Figure 13) show a predominantly linear arrangement, consistent with findings across the WEC optimization literature. Ref. [3] noted that linear

arrangements emerge frequently as optimal, attributing this to reduced hydrodynamic interference and simplified cable routing. Ref. [13] found arrow-shaped layouts optimal under real bathymetric conditions, which partially aligns with our elongated layouts that follow wave power gradients. Similar patterns were also observed by [7], who found that optimal layouts that prefer maximum power formed single lines perpendicular to the predominant wave direction.

However, our results reveal an important nuance absent from previous studies: the definition of "optimal" depends on whether one prioritizes absolute minimum cost or statistical reproducibility. The absolute minima (Figure 13, top row) represent singular solutions that the GA found in specific executions, while the K-means-derived *star-layouts* (bottom row) are those that emerge consistently across multiple executions. For practical deployment, the latter may be preferable despite a marginally higher cost (1.3–2.1% difference), as they indicate robust optima less sensitive to initial conditions and parameter choices. Structurally, the absolute minima tend toward more linear arrangements, while the *star-layouts* follow more closely the spatial distribution of wave power, adapting to the shape of the high-energy zones (Figure 13).

5.2.3. Solution Multiplicity

The identification of multiple solution families through K-means clustering represents a methodological contribution that complements traditional single-optimum approaches. While [3,19] focused on identifying single optimal layouts, our clustering analysis reveals that the optimization landscape contains 2–4 distinct basins of attraction with silhouette scores between 0.627 and 0.855, indicating well-separated solution families across the three cost scenarios.

This multiplicity of near-optimal solutions has been observed in related fields but rarely characterized systematically. In wind farm optimization, Ref. [32] noted that genetic algorithms converge to different local optima across executions. More recently, Ref. [33] applied clustering to wind farm layouts but focused on wake effects rather than cost optimization. Ref. [6] examined minimum separation distances in WEC arrays but did not characterize solution families. Our K-means approach provides a transferable framework for quantifying solution variability in marine energy applications.

5.3. Solution Robustness and Optimization Performance

Beyond the cost component analysis, our systematic parameter study revealed important insights about optimization robustness in bathymetry-influenced landscapes.

The number of solution families decreased monotonically from 4 to 3 to 2 as cost components were added, indicating that infrastructure constraints reduce the feasible solution space. This constraint-driven convergence has a dual interpretation: it reduces design flexibility but simultaneously improves optimization robustness by sharpening the attraction basins of the GA. For project developers, fewer but more clearly defined solution families simplify decision-making.

The practical value of maintaining multiple solution families extends beyond statistical robustness. Often, developers face constraints not captured by LCOE models: environmental restrictions may prohibit certain areas, navigation corridors must be avoided, visual impact concerns may eliminate near-shore options, and phased deployment plans may favor expandable layouts. Having 2–4 near-optimal alternatives with comparable LCOE provides flexibility to accommodate these real-world factors without significant economic penalty.

Regarding GA parameters, bathymetry-influenced landscapes benefit from higher mutation rates (0.05–0.10) than typical applications (0.01–0.02). In multimodal fitness land-

scapes, higher mutation rates increase the probability of escaping local optima by enabling simultaneous changes across multiple variables, whereas the standard rate $p_m = 1/l$ is theoretically suboptimal for such landscapes [28,29]. Complex bathymetries can create multiple local power maxima that can trap algorithms with insufficient exploration capacity, constituting precisely this type of multimodal landscape. Higher mutation rates sacrifice convergence speed for improved global search, a worthwhile trade-off given that WEC park planning operates on development timescales of months to years rather than real-time optimization.

The recommendation for multiple executions ($\geq$100) emerges directly from the clustering analysis. With fewer executions, the sampling of solution families becomes unreliable, increasing the risk of choosing layouts that represent local rather than global optima. The computational overhead of 100 executions (approximately 2–4 h on standard hardware for our 10-device park) is negligible compared to the scale of the investment decisions these optimizations inform.

5.4. Limitations and Scope

Before generalizing these findings, several limitations warrant discussion. At sites with more variable or multidirectional wave climates, directional variability could affect optimal park layouts more strongly than at directionally stable sites like Todos Santos Bay [34]. Beyond directional variability, wave loading, resonance phenomena, and hydrodynamic interactions in multi-body arrays are highly sensitive to wave complexity, including transient focused wave groups and topographic effects [35–38]. In particular, bathymetrically complex coastal zones (such as the study site here) can shift resonant frequencies and amplify structural forces on closely spaced structures in ways not captured by regular or monochromatic wave assumptions [35,36]. Incorporating transient, nonlinear wave representations in future hydrodynamic analyses would strengthen the theoretical foundation of WEC park optimization in variable-bathymetry environments.

Hydrodynamic interactions between WEC devices were not modeled: park power is computed as the sum of the SWAN-derived available wave power at each device node independently, which is equivalent to assuming an interaction factor of unity. Studies using full hydrodynamic coupling show that interaction effects become small (a few percent) only once device separation exceeds approximately 10–20 body diameters [25]; since our minimum spacing constraint (Equation (4)) is set at $3D$, some device pairs in the optimized layouts may exhibit non-negligible interactions. Full hydrodynamic models [19,23,39] that account for nonlinear and transient wave excitation, including the gap resonance effects documented between closely spaced floating bodies [37,38], should be incorporated in future work to quantify this effect on the identified layouts. As a first-order quantitative estimate based on the pairwise approximation of [25] applied to the [40] numerical data, the array interaction factor for the three *star-layouts* is weakly constructive ($q^{\star}_{\text{park}} \in [1.005, 1.018]$, see Appendix A).

Additionally, the LCOE model omits factors such as maintenance access, environmental permitting costs, and grid connection capacity constraints; these are expected to play a significant role in detailed feasibility studies where site-specific regulatory or logistical constraints are decisive.

Two further model-fidelity caveats deserve explicit mention here. First, the device efficiency $\eta = 1$ adopted in the LCOE objective (Section 3.2) is a known idealization; an LCOE sensitivity envelope over realistic η values is reported in Appendix A, and the qualitative cost-component hierarchy of the manuscript is preserved across that envelope. Second, we did not perform site-specific SWAN validation in the present study; the wave power field used in the optimization relies on the previously published SNL-SWAN hindcast of [15],

and site-specific validation against in situ measurements would strengthen confidence in the absolute LCOE values reported here, although it would not be expected to alter the relative cost-component hierarchy that is the principal finding of this study.

Most importantly, the magnitude of the bathymetry-dependent mooring contribution is conditioned by the range of depth gradients considered. At Todos Santos Bay, this contribution is +16.0% in LCOE with a 151 m park-center reorganization (Table 6). At sites with steeper bathymetric gradients, or where floating WEC technologies with depth-sensitive mooring systems are considered, the bathymetry cost component would likely become more significant; the analysis framework presented here can be applied to these cases.

Despite these limitations, the cost-component hierarchy we observe (cable approximately three times more impactful than bathymetry-dependent mooring, with both contributions material in absolute terms) provides practical guidance for the early-stage techno-economic assessment of WEC parks at near-shore sites with moderate depth gradients. The finding is robust across all configurations tested, lending confidence to its generalizability within the range of depth gradients studied.

5.5. Implications for Wave Energy Development

These findings have direct implications for the emerging wave energy industry at multiple stages of project development [2].

For preliminary site assessment, our results imply that both cable routing and bathymetry-dependent mooring costs should be incorporated from the earliest stages of WEC park planning. The combined infrastructure cost contribution of more than 70% to LCOE found here (Tables 5 and 6) makes flat-bathymetry simplifications untenable for techno-economic estimates intended to inform investment decisions, even at sites with the moderate depth gradients of Todos Santos Bay.

For site selection strategy, the larger cable contribution implies that sites with existing electrical infrastructure (decommissioned offshore platforms, coastal industrial facilities, or areas with submarine cable landfalls) may offer significant advantages over remote high-energy locations [41]. Reductions in shore distance can offset meaningful reductions in wave-power availability when ranking candidate sites in regional resource assessments. At sites with depth gradients comparable to or steeper than Todos Santos Bay, this trade-off should be evaluated jointly with the bathymetry-dependent mooring cost identified here as a nontrivial second contribution.

For optimization methodology, our results advocate for a portfolio approach rather than seeking a single optimum. The existence of 2–4 near-optimal layout families per scenario suggests that WEC park planning should identify and characterize multiple viable layouts, allowing subsequent selection based on constraints that emerge during permitting, financing, and detailed engineering phases. This approach aligns with decision-making under uncertainty frameworks increasingly adopted in offshore renewable energy development [7].

Finally, the transferability of these conclusions to other WEC technologies requires validation. Point absorbers with catenary moorings, as modeled here, have moderate depth sensitivity (see Table 6). Oscillating water columns with bottom-founded structures, tension-leg platforms, or floating attenuators may exhibit different cost hierarchies [2,25]. We recommend that technology developers conduct similar sensitivity analyses for their specific device configurations before adopting simplified bathymetry assumptions.

6. Conclusions

This study quantified how submarine cable costs and bathymetry-dependent mooring costs affect WEC park optimization using real data from Todos Santos Bay, Mexico. The

central finding is that both infrastructure cost components—submarine cables and depth-dependent mooring lines—substantially influence LCOE and the best-found park layouts. Cable costs are the larger contribution, but bathymetry-dependent mooring costs are also material: this directly contradicts the common literature practice of using flat-bathymetry approximations and cable-only cost models for techno-economic assessment of WEC parks at sites with nontrivial depth variation.

Three main findings emerge from the systematic analysis of 48 configurations, with 100 independent GA executions for each configuration:

Both cable and bathymetry-dependent mooring costs are material LCOE drivers. Including submarine cable costs raised LCOE by 52.2% (172 m park-center shift); adding bathymetry-dependent mooring costs raised LCOE by an additional 16.0% (151 m further shift), with cable being approximately three times more impactful than mooring. The cumulative infrastructure cost contribution exceeds 70% of LCOE relative to the no-infrastructure baseline, demonstrating that flat-bathymetry simplifications systematically miss a substantial fraction of the cost budget.

Cost components progressively constrain solution diversity. K-means clustering identified 2–4 distinct layout families per scenario, with the number decreasing monotonically as cost components are added ($K = 4 \rightarrow 3 \rightarrow 2$). This progression indicates that infrastructure constraints eliminate marginally viable solutions and sharpen the convergence of the GA toward a smaller set of robust layouts.

Multimodal landscapes require adjusted GA parameters. Mutation rates of 0.05–0.10 outperformed standard values (0.01–0.02) in terms of achieved LCOE [28,29]. Multiple executions ($\geq$100) proved essential for characterizing solution families and ensuring robust convergence.

These findings are bounded by the moderate depth gradient of Todos Santos Bay. Sites with steeper gradients or different WEC technologies may exhibit different cost hierarchies and warrant specific evaluation.

Recommendations

For practitioners, three actionable recommendations emerge from this work. First, include cable costs from the earliest planning stages: their omission can lead to substantial underestimation of LCOE (+52.2% in this study) even when the optimized park location remains within the same wave-focusing region. Second, include bathymetry-dependent mooring costs even at sites with moderate depth gradients: in this study, they accounted for an additional 16.0% of LCOE and a 151 m park reorganization, contradicting the common practice of using flat-bathymetry approximations for preliminary techno-economic assessment. Third, adopt a portfolio approach to optimization, characterizing multiple layout families rather than seeking a single optimum, to preserve flexibility for constraints that emerge during project development.

Future work should apply this framework at sites with steeper bathymetric gradients to test the transferability of the cost-hierarchy findings, extend the cost model to floating WEC technologies where mooring scales more strongly with depth, and incorporate explicit hydrodynamic interactions through a precomputed q-factor matrix or full boundary-element coupling.

Author Contributions: Conceptualization, E.S.-O., H.G.-N. and E.G.-L.; methodology, E.S.-O.; software, E.S.-O., H.G.-N. and E.G.-L.; validation, E.S.-O., H.G.-N. and E.G.-L.; formal analysis, E.S.-O.; investigation, E.S.-O.; resources, H.G.-N.; data curation, E.S.-O., H.G.-N. and E.G.-L.; writing—original draft preparation, E.S.-O.; writing—review and editing, H.G.-N., E.G.-L., M.G.V.-Z. and G.G.M.; visualization, E.S.-O.; supervision, H.G.-N. and E.G.-L.; project administration, H.G.-N.; funding acquisition, H.G.-N. All authors have read and agreed to the published version of the manuscript.

Funding: The authors are grateful to the National Council of Science and Technology (CONACyT) for the PhD grant assigned to E.S.-O.

Institutional Review Board Statement: Not applicable.

Informed Consent Statement: Not applicable.

Data Availability Statement: The data presented in this study are available upon request from the corresponding author.

Acknowledgments: The authors thank Aurélien Babarit (École Centrale de Nantes/CNRS) for kindly providing the numerical data underlying Figure 14 of [40], which were used to construct the pairwise q-factor envelope and the q^*_{park} sensitivity tables presented in Appendix A. During the preparation of this manuscript, the authors used Claude Code (Anthropic, Claude-Sonnet-4.6) to translate the draft text from Spanish to English, correct spelling and grammar, and improve sentence structure. The authors have reviewed and edited the output and take full responsibility for the content of this publication.

Conflicts of Interest: Gabriel García Medina was employed by the Natural Systems Design, Seattle, USA. The remaining authors declare that the research was conducted in the absence of any commercial or financial relationships that could be construed as a potential conflict of interest.

Abbreviations

The following abbreviations are used in this manuscript:

AEP	Annual Energy Production
CapEx	Capital Expenditure
GA	Genetic Algorithm
LCOE	Levelized Cost of Energy
OpEx	Operational Expenditure
SWAN	Simulating Waves Nearshore
WEC	Wave Energy Converter

Appendix A. LCOE Sensitivity to Device Efficiency η and Park Interaction Factor q_{park}

This appendix presents the sensitivity of the levelized cost of energy (LCOE) to two assumptions adopted in the main analysis: (i) a device efficiency of $\eta = 1$ (Section 3, Equation (9)), and (ii) an array interaction factor of $q_{\text{park}} = 1$ implicit in the additive park-power model (Section 5, Limitations).

A realistic range for η is taken to be $\eta \in \{0.2, 0.3, 0.4\}$, covering the typical capture-width ratio of heaving point absorbers reported by [42] (mean 0.16, best-in-class 0.35–0.40 across $n = 56$ technologies in the CWR database). The literature-based envelope for the array interaction factor is taken to be $q_{\text{park}} \in \{0.90, 0.95, 1.00, 1.05, 1.10\}$, consistent with the $\pm 10\%$ range reported by [43] for arrays of $N < 10$ heaving converters in irregular seas; the optimized arrangements of [19] reach $q_{\text{park}} \approx 1.05$.

For each scenario, a layout-specific $q^\star_{\text{park}}$ is computed from the *star-layout* WEC positions using the pairwise approximation of [25]:

$$q^\star_{\text{park}} = 1 + \frac{2}{N} \sum_{i<j} \left(q_{ij}(d_{ij}, \theta_{ij}) - 1 \right), \tag{A1}$$

where d_{ij} is the inter-device distance, and θ_{ij} is the angle between the line i–j and the dominant wave direction (354° at Todos Santos Bay, Table 1). The pairwise factors $q_{ij}(d, \theta)$ are interpolated from the numerical data underlying Figure 14 of [40] (heaving WEC pair, irregular seas). The resulting layout-specific values are $q^\star_{\text{park}} = 1.0078$ (CableNoDeepNo), 1.0047 (CableSiDeepNo), and 1.0175 (CableSiDeepSi), all weakly constructive and within

the literature envelope. None of the 45 pairs in each scenario falls below the 100 m floor of the Babarit data, so no extrapolation is required.

Each cell of Tables A1–A3 reports the LCOE under the analytical scaling $\mathrm{LCOE}(\eta, q_{\mathrm{park}}) = \mathrm{LCOE}_{\mathrm{baseline}}/(\eta \cdot q_{\mathrm{park}})$, with the row for the layout-specific $q^{\star}_{\mathrm{park}}$ shaded. The qualitative cost-component hierarchy (with cable being approximately three times more impactful than bathymetry-dependent mooring, while both contributions remain material) is preserved across the full $(\eta, q_{\mathrm{park}})$ envelope, confirming that the conclusions of this study are robust to the two assumptions tested.

Table A1. LCOE (EUR/MWh) envelope for the scenario CableNoDeepNo (baseline 153). The layout-specific $q^{\star}_{\mathrm{park}} = 1.0078$ row is shaded.

q_{park}	$\eta = 0.2$	$\eta = 0.3$	$\eta = 0.4$
0.90	852	568	426
0.95	807	538	404
1.00	767	511	383
1.0078	761	507	380
1.05	730	487	365
1.10	697	465	349

Table A2. LCOE (EUR/MWh) envelope for the scenario CableSiDeepNo (baseline 233). The layout-specific $q^{\star}_{\mathrm{park}} = 1.0047$ row is shaded.

q_{park}	$\eta = 0.2$	$\eta = 0.3$	$\eta = 0.4$
0.90	1297	864	648
0.95	1228	819	614
1.00	1167	778	583
1.0047	1161	774	581
1.05	1111	741	556
1.10	1061	707	530

Table A3. LCOE (EUR/MWh) envelope for the scenario CableSiDeepSi (baseline 271). The layout-specific $q^{\star}_{\mathrm{park}} = 1.0175$ row is shaded.

q_{park}	$\eta = 0.2$	$\eta = 0.3$	$\eta = 0.4$
0.90	1504	1003	752
0.95	1425	950	713
1.00	1354	903	677
1.0175	1331	887	665
1.05	1290	860	645
1.10	1231	821	615

Appendix B. LCOE Sensitivity to the Mooring Cost Rate and the Discount Rate

This appendix presents the sensitivity of the LCOE to two cost-model parameters that enter the LCOE objective but do not affect the optimization itself: the bathymetry-dependent mooring cost rate (Equation (11)) and the discount rate r (Equation (1)).

The mooring cost contribution to LCOE is obtained from the difference between the CableSiDeepSi scenario (cable plus bathymetry-dependent mooring) and the CableSiDeepNo scenario (cable only), and scales linearly with the rate because, for a fixed *star-layout*, the mooring cost per device is the rate multiplied by a layout-dependent constant $(4 \cdot \mathrm{Depth}(x_i, y_i))$. Table A4 reports the LCOE under three rates (200, 400, and 600 EUR/m), corresponding to the ±50% range requested by the reviewer. At the lower bound of the sensitivity range, the mooring contribution drops to +8.0% relative to the

cable-only baseline; at the upper bound, it rises to +24.1%. In all three cases, the cable contribution (+52.2%) remains the larger of the two infrastructure cost components, and the qualitative cost-component hierarchy of the manuscript is preserved.

Table A4. LCOE sensitivity (EUR/MWh) of the three cost scenarios to the bathymetry-dependent mooring cost rate. The baseline rate of 400 EUR/m (after [12]) is varied by ±50%. Mooring costs enter only the CableSiDeepSi scenario; the other two scenarios are unchanged. The mooring contribution scales linearly with the rate because the WEC positions in the *star-layout* are fixed across the sensitivity analysis. The shaded row marks the baseline.

Rate (EUR/m)	CableNoDeepNo (EUR/MWh)	CableSiDeepNo (EUR/MWh)	CableSiDeepSi (EUR/MWh)	Δ_{mooring} (EUR/MWh)	Mooring Contribution (% over CableSiDeepNo)
200 (−50%)	153.36	233.38	252.09	+18.72	+8.0%
400 (+0%)	153.36	233.38	270.81	+37.43	+16.0%
600 (+50%)	153.36	233.38	289.52	+56.15	+24.1%

The discount rate r enters the LCOE expression through both the numerator (present value of OpEx) and the denominator (present value of AEP). The relative ranking of the three cost scenarios and the percentage differences between them are robust to changes in r within typical project-finance ranges ($r \in [3\%, 7\%]$): all three scenarios share the same CapEx/OpEx structure and the same project lifetime, so the capital recovery factor $r/(1-(1+r)^{-L})$ that scales the CapEx contribution to LCOE acts as a common multiplier across scenarios. Therefore, a discount-rate sensitivity changes the absolute LCOE values but does not alter the cost-component hierarchy that constitutes the principal finding of this study; we have not reported a numerical r-sensitivity table because it would not add information beyond a uniform rescaling of all three scenarios.

References

1. Falnes, J. A review of wave-energy extraction. *Mar. Struct.* **2007**, *20*, 185–201. [CrossRef]
2. Falcão, A.F.d.O. Wave energy utilization: A review of the technologies. *Renew. Sustain. Energy Rev.* **2010**, *14*, 899–918. [CrossRef]
3. Göteman, M.; Giassi, M.; Engström, J.; Isberg, J. Advances and Challenges in Wave Energy Park Optimization—A Review. *Front. Energy Res.* **2020**, *8*, 26. [CrossRef]
4. Teixeira-Duarte, F.; Clemente, D.; Giannini, G.; Rosa-Santos, P.; Taveira-Pinto, F. Review on layout optimization strategies of offshore parks for wave energy converters. *Renew. Sustain. Energy Rev.* **2022**, *163*, 112513. [CrossRef]
5. Giassi, M.; Castellucci, V.; Engström, J.; Göteman, M. An economical cost function for the optimization of wave energy converter arrays. In *Proceedings of the 29th International Ocean and Polar Engineering Conference*; Paper No. ISOPE-I-19-230; ISOPE: Honolulu, HI, USA, 2019; pp. 3546–3552.
6. Sharp, C.; DuPont, B. Wave energy converter array optimization: A genetic algorithm approach and minimum separation distance study. *Ocean Eng.* **2018**, *163*, 148–156. [CrossRef]
7. David, D.R.; Kurniawan, A.; Wolgamot, H.; Hansen, J.E.; Rijnsdorp, D.; Lowe, R. Nearshore submerged wave farm optimisation: A multi-objective approach. *Appl. Ocean Res.* **2022**, *124*, 103225. [CrossRef]
8. Bergström, K.; Göteman, M. Comprehensive multi-objective optimisation of wave power parks. In *Innovations in Renewable Energies Offshore, Proceedings of the 6th International Conference on Renewable Energies Offshore, RENEW 2024*; CRC Press/Balkema: Boca Raton, FL, USA, 2025; pp. 295–305. [CrossRef]
9. Izquierdo-Pérez, J.; Brentan, B.M.; Izquierdo, J.; Clausen, N.E.; Pegalajar-Jurado, A.; Ebsen, N. Layout optimization process to minimize the cost of energy of an offshore floating hybrid wind-wave farm. *Processes* **2020**, *8*, 139. [CrossRef]
10. Mercadé Ruiz, P.; Nava, V.; Topper, M.B.; Minguela, P.R.; Ferri, F.; Kofoed, J.P. Layout optimisation of wave energy converter arrays. *Energies* **2017**, *10*, 1262. [CrossRef]
11. Vazquez, A.; Iglesias, G. LCOE (levelised cost of energy) mapping: A new geospatial tool for tidal stream energy. *Energy* **2015**, *91*, 192–201. [CrossRef]

12. O'Connell, R.; Kamidelivand, M.; Furlong, R.; Guerrini, M.; Cullinane, M.; Murphy, J. An advanced geospatial assessment of the Levelised cost of energy (LCOE) for wave farms in Irish and western UK waters. *Renew. Energy* **2024**, *221*, 119864. [CrossRef]
13. López-Ruiz, A.; Bergillos, R.J.; Raffo-Caballero, J.M.; Ortega-Sánchez, M. Towards an optimum design of wave energy converter arrays through an integrated approach of life cycle performance and operational capacity. *Appl. Energy* **2018**, *209*, 20–32. [CrossRef]
14. Bozzi, S.; Giassi, M.; Miquel, A.; Antonini, A.; Bizzozero, F.; Gruosso, G.; Archetti, R.; Passoni, G. Wave energy farm design in real wave climates: The Italian offshore. *Energy* **2017**, *122*, 378–389. [CrossRef]
15. Gorr-Pozzi, E.; García-Nava, H.; Larrañaga, M.; Jaramillo-Torres, M.G.; Verduzco-Zapata, M.G. Wave energy resource harnessing assessment in a subtropical coastal region of the pacific. *J. Mar. Sci. Eng.* **2021**, *9*, 1264. [CrossRef]
16. Sánchez, A.; Mendoza, E. Wave energy converter farm feasibility assessment in southwest Baja California, Mexico. *Renew. Energy* **2024**, *227*, 120589. [CrossRef]
17. Pozzi, G.; Nelson, E. Focalización del Oleaje con Estructuras Sumergidas para Fines Recreativos en Playa Hermosa, Baja California. Ph.D. Thesis, Universidad Autónoma de Baja California, Ensenada, Mexico, 2015.
18. Haupt, R.L.; Haupt, S.E. *Practical Genetic Algorithms*; Wiley-Blackwell: Hoboken, NJ, USA, 2004; pp. 1–253. [CrossRef]
19. Giassi, M.; Göteman, M. Layout design of wave energy parks by a genetic algorithm. *Ocean Eng.* **2018**, *154*, 252–261. [CrossRef]
20. MacQueen, J. Some methods for classification and analysis of multivariate observations. In *Proceedings of the Fifth Berkeley Symposium on Mathematical Statistics and Probability*; University of California Press: Oakland, CA, USA, 1967; Volume 1, pp. 281–297.
21. Giassi, M.; Castellucci, V.; Göteman, M. Economical layout optimization of wave energy parks clustered in electrical subsystems. *Appl. Ocean Res.* **2020**, *101*, 102274. [CrossRef]
22. Guo, C.; Sheng, W.; De Silva, D.G.; Aggidis, G. A Review of the Levelized Cost of Wave Energy Based on a Techno-Economic Model. *Energies* **2023**, *16*, 2144. [CrossRef]
23. Loukogeorgaki, E.; Michailides, C.; Lavidas, G.; Chatjigeorgiou, I.K. Layout optimization of heaving Wave Energy Converters linear arrays in front of a vertical wall. *Renew. Energy* **2021**, *179*, 189–203. [CrossRef]
24. Booij, N.; Ris, R.; Holthuijsen, L. A third-generation wave model for coastal regions: 1. Model description and validation. *J. Geophys. Res. Ocean.* **1999**, *104*, 7649–7666. [CrossRef]
25. Babarit, A. On the park effect in arrays of oscillating wave energy converters. *Renew. Energy* **2013**, *58*, 68–78. [CrossRef]
26. Goldberg, D.E. *Genetic Algorithms in Search, Optimization and Machine Learning*; Addison-Wesley: Reading, MA, USA, 1989.
27. Rousseeuw, P.J. Silhouettes: A graphical aid to the interpretation and validation of cluster analysis. *J. Comput. Appl. Math.* **1987**, *20*, 53–65. [CrossRef]
28. Bäck, T. Optimal mutation rates in genetic search. In Proceedings of the 5th International Conference on Genetic Algorithms, San Francisco, CA, USA, 1 June 1993; Volume 28, pp. 2–8.
29. Črepinšek, M.; Liu, S.H.; Mernik, M. Exploration and exploitation in evolutionary algorithms: A survey. *ACM Comput. Surv.* **2013**, *45*, 35. [CrossRef]
30. Eiben, A.E.; Smith, J.E. 9 Working with Evolutionary Algorithms. In *Introduction to Evolutionary Computing*; Springer: Berlin/Heidelberg, Germany, 2015; pp. 147–163.
31. Teixeira-Duarte, F.; Rosa-Santos, P.; Taveira-Pinto, F. Multi-objective optimization of co-located wave-wind farm layouts supported by genetic algorithms and numerical models. *Renew. Energy* **2025**, *241*, 122362. [CrossRef]
32. Mosetti, G.; Poloni, C.; Diviacco, B. Optimization of wind turbine positioning in large windfarms by means of a genetic algorithm. *J. Wind. Eng. Ind. Aerodyn.* **1994**, *51*, 105–116. [CrossRef]
33. Feng, J.; Shen, W.Z. Solving the wind farm layout optimization problem using random search algorithm. *Renew. Energy* **2015**, *78*, 182–192. [CrossRef]
34. Göteman, M.; Giassi, M.; McNatt, C. Wave energy park interactions in short-crested waves. In Proceedings of the 33rd Intl. Workshop on Water Waves and Floating Bodies, Guidel-Plagues, France, 4–7 April 2018.
35. Gao, J.; He, Z.; Zang, J.; Chen, Q.; Ding, H.; Wang, G. Topographic effects on wave resonance in the narrow gap between fixed box and vertical wall. *Ocean Eng.* **2019**, *180*, 97–107. [CrossRef]
36. Gao, J.; He, Z.; Zang, J.; Chen, Q.; Ding, H.; Wang, G. Numerical investigations of wave loads on fixed box in front of vertical wall with a narrow gap under wave actions. *Ocean Eng.* **2020**, *206*, 107323. [CrossRef]
37. Gao, J.; Mi, C.; Song, Z.; Liu, Y. Transient gap resonance between two closely-spaced boxes triggered by nonlinear focused wave groups. *Ocean Eng.* **2024**, *305*, 117938. [CrossRef]
38. Mi, C.; Gao, J.; Song, Z.; Liu, Y. Hydrodynamic wave forces on two side-by-side barges subjected to nonlinear focused wave groups. *Ocean Eng.* **2025**, *317*, 120056. [CrossRef]
39. Child, B.F.; Venugopal, V. Optimal configurations of wave energy device arrays. *Ocean Eng.* **2010**, *37*, 1402–1417. [CrossRef]
40. Babarit, A. Impact of long separating distances on the energy production of two interacting wave energy converters. *Ocean Eng.* **2010**, *37*, 718–729. [CrossRef]
41. Sjolte, J.; Tjensvoll, G.; Molinas, M. Power collection from wave energy farms. *Appl. Sci.* **2013**, *3*, 420–436. [CrossRef]

42. Babarit, A. A database of capture width ratio of wave energy converters. *Renew. Energy* **2015**, *80*, 610–628. [CrossRef]
43. Borgarino, B.; Babarit, A.; Ferrant, P. Impact of wave interactions effects on energy absorption in large arrays of wave energy converters. *Ocean Eng.* **2012**, *41*, 79–88. [CrossRef]